Quarterly Reviews of Biophysics 9, 3 (1976), pp. 311–375.
Printed in Great Britain

Visual control of orientation behaviour in the fly

Part I. A quantitative analysis

WERNER REICHARDT AND TOMASO POGGIO
Max-Planck-Institut für biologische Kybernetik
D 7400 Tübingen (Germany)

1 INTRODUCTION 312

2 FLIGHT ORIENTATION BEHAVIOUR 315

3 PHENOMENOLOGICAL THEORY 318
- 3.1. *Spontaneous behaviour* 319
- 3.2. *Visually induced behaviour* 320
- 3.3. *The phenomenological equation* 321

4 SIMPLE APPLICATIONS OF THE THEORY 328
- 4.1. *A linear approach* 328
- 4.2. *Fixation* 329
- 4.3. *Role of movement- and position-dependent responses* 331

5 THE MATHEMATICS OF THE THEORY 334

6 DESCRIPTION OF TRACKING AND ORIENTATION 340
- 6.1. *Tracking of a target moving with constant angular velocity* 340
- 6.2. *Tracking of an object in front of a background* 341
- 6.3. *Antifixation* 343
- 6.4. *Patterns consisting of two identical elements* 345
- 6.5. *Tracking of a randomly moving object* 347
- 6.6. *Is the theory valid under free flight conditions?* 349

7 MOVEMENT AND POSITION RESPONSES ASSOCIATED TO ARBITRARY PATTERNS 351
7.1. *Properties of the fly's response* 351
7.2. *The superposition 'rule'* 354
7.3. *Restrictions of the superposition 'rule'* 355
8 DISCUSSION 358
8.1. *The central thesis of the theory* 358
8.2. *Separation of the fly's response* 358
8.3. *The role of the 'noise' N(t)* 361
8.4. *Validity of the theory and possible extensions* 364
8.5. *Phase transitions and Gestalt* 368
9 APPENDIX: ANATOMICAL AND PHYSIOLOGICAL BACKGROUND 370
10 REFERENCES (SEE PART II, pp. 428–438)

1. INTRODUCTION

An understanding of sensory information processing in the nervous system will probably require investigations with a variety of 'model' systems at different levels of complexity.

Our choice of a suitable model system was constrained by two conflicting requirements: on one hand the information processing properties of the system should be rather complex, on the other hand the system should be amenable to a quantitative analysis. In this sense the fly represents a compromise.

In these two papers we explore how optical information is processed by the fly's visual system. Our objective is to unravel the logical organization of the fly's visual system and its underlying functional and computational principles. Our approach is at a highly integrative level. There are different levels of analysing and 'understanding' complex systems, like a brain or a sophisticated computer. At the first, strictly 'phenomenological' level, one investigates the overall function of the system, its input–output behaviour, and its logical organization. At the second level, the functional principles of the subsystems are the object of the analysis. At the third level one studies individual components and detailed

circuitry. A reductionist approach can certainly reduce a complex behaviour to fundamental laws at the cellular or even molecular levels. However, this does not imply the validity of the converse, constructionist approach. The behaviour of a complex system, composed of many elements, cannot be easily understood in terms of a simple extrapolation of the properties of its components. New properties appear and their understanding requires an independent approach which is as fundamental in its nature as any other. There are of course causal and logical relationships between these levels, but knowledge at one level might be of little help at any other one. However, an understanding of the functional property at higher levels might help to develop approaches at lower levels. In physics, for instance, thermodynamics which is, in a sense, analogous to our first level, represents historically the first stage in the study of matter. A description in terms of molecular structures appears almost always afterwards. In fact, generally still too little is known about the details of any nervous system in order to model it completely enough to predict actual behaviour. Consequently, a direct study of the overall behaviour should prove more fruitful.

Our approach towards an understanding of the visual control system of the fly reflects the above view. Although we will briefly outline some histological and electrophysiological data, we are primarily concerned with the first two levels, defined earlier.

Part I outlines a phenomenological theory of the fly's visual orientation behaviour based on experimental evidence. This theory describes and predicts, at the first level, a rather complex behaviour in terms of some simple computations which are performed by nervous interactions on the visual input. Part II characterizes, at the second level, the functional properties of the interactions underlying the computations. We maintain that the two levels of analysis, in these two papers, cannot simply follow from single cell recordings or from histology. Furthermore, they are bound to be, at least in a 'historical' sense, a prerequisite to any full understanding at the 'circuitry' level. Of course, the ultimate goal of our research is to relate function to structure and there is no doubt that neurophysiology and histology are the basic tools at the third, 'cellular', level.

We believe that at least three main arguments, which arise from our investigation, may be generally applicable to other areas of neurophysiology. The first argument is that a quantitative phenomenological description of the 'behaviour' of a nervous system is as necessary as

studies of its anatomy and cell physiology. Equally important is a characterization of the functional and computational principles which are involved. This aspect, relatively simple in the fly (Part II), may become much more complex in other cases (see, for instance, Marr, 1975).† The second argument maintains that the co-operative superposition of local, simple computations or interactions in the nervous system, may lead to a completely new and highly complicated behaviour. Thus, inferences about the system information processing, based on knowledge of local computations, may be near to impossible. The third argument concerns the concept of feature and feature-detectors which has played an important role in sensory physiology since the original proposal of Lettvin *et al.* (1959). We believe that a computational point of view may be more fruitful than the 'detector' approach. For the simple parallel, non-symbolic preprocessing, studied in these two papers, we propose a specific canonical classification of the computations performed by the network in terms of the underlying functional interactions (Part II). A description of information processing at higher levels will certainly require a more sophisticated approach (see, for instance, Winston, 1975). However, preprocessing of information in biological systems may be usefully characterized in terms of the functional language, outlined in Part II of this review. We maintain that this language represents a conceptual model of information processing which is flexible enough not to restrict the interpretation of neurophysiological data at an early stage of understanding.

We summarize here the organization of the first paper. In chapter 2 we describe the flight orientation behaviour of the fly. In chapter 3 the phenomenological equation of the flight orientation behaviour is derived, while chapter 4 presents some elementary applications of the theory. Chapter 5 deals with mathematical aspects of the phenomenological theory. Various tracking and orientation situations can be quantitatively described by the theory, as shown by chapter 6. Chapter 7 deals with the problem of deriving the fly's movement and position computations for arbitrary patterns and shows the necessity of the interaction approach presented in Part II. Various aspects of the phenomenological theory are discussed in the last chapter. An appendix briefly outlines the anatomy and the physiology of the fly's visual system.

† References are combined with those of Part II, pp. 428–438.

2. Flight orientation behaviour

The flight behaviour of houseflies demonstrates an elaborate visual control system. Houseflies perceive motion relative to the environment and thereby stabilize their flight course; they locate and fly towards prominent objects; they are able to track moving targets and to chase other flies; they discriminate or prefer some specific visual patterns; they can in some cases separate a visual texture into 'figure' and 'ground'. A quantitative analysis of this orientation behaviour represents the main subject of Part I. In this chapter we introduce some elementary kinematics and dynamics of the flight behaviour.

In free flight, a fly has three rotational and three translational degrees of freedom. Moreover, the neck (cervix) enables the head to be rotated through small angles relative to the body. The studies of the flight orientation behaviour reviewed in this paper are restricted to one rotational and one translational degree of freedom. In most cases the head was also artificially fixed to the thorax, thus eliminating the neck movements. Under this condition the fly's body axis also provides a precise measure of the direction of the head. Several arguments suggest that blocking these degrees of freedom – including movements of the head – does not essentially affect the orientation behaviour (Land & Collett, 1974; Geiger, in preparation). This point will be briefly discussed later.

Imagine a fly flying freely in a room. Fig. 1 shows a suitable angular coordinate system, which describes the angular position of the fly on the horizontal plane. α_f designates the instantaneous direction of flight with respect to an arbitrary zero-direction, α_p the instantaneous angular position of an object which the fly may or may not track. The angle $\psi = \alpha_p - \alpha_f$ is referred to as the *error angle* and represents the angular position of the object with respect to the coordinate system of the fly. When the head is fixed to the thorax $\psi(t)$ also represents the location of the image of the object on the retina of the fly at a particular instant. When $\alpha_f = \alpha_p$ the fly's long axis points towards the object ($\psi = 0$).

The free flight situation represented in Fig. 1 can be summarized by the signal flow diagram of Fig. 2(*a*). The 'fly' has been 'split' into two boxes, one describing the visual input–torque output relation, the other representing the flight dynamics. In fact, a rotation of the fly around its vertical axis depends on the torque $F(t)$, generated by the wings. It has been shown (Reichardt & Wenking, 1969; Reichardt, 1973; Land &

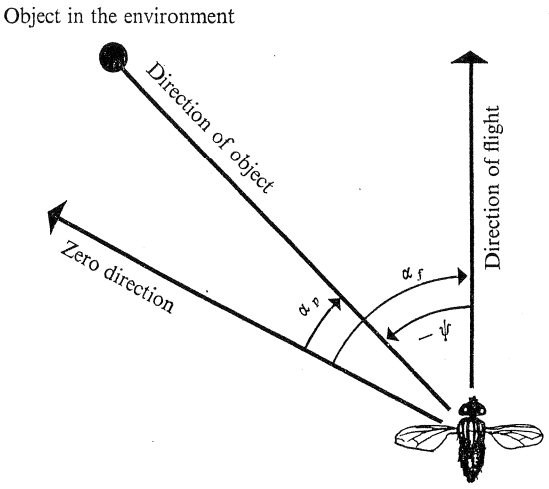

Fig. 1. Angular coordinate system describing the fly's rotational degree of freedom around the vertical axis. $\alpha_p(t)$ designates the angle between an arbitrary zero direction and the direction of an object in the fly's environment; $\alpha_f(t)$ the angle between the zero direction and the fly's direction of flight; $\psi(t) = \alpha_p(t) - \alpha_f(t)$ is the 'error angle' between the fly's direction of flight and the object. It represents the location of the object on the retina of the fly.

Collett, 1974) that the free flight dynamics of rotation is well approximated by

$$\Theta\ddot{\alpha}_f(t) + k\dot{\alpha}_f(t) = F(t), \tag{2.1}$$

where $\Theta = 1{\cdot}5 \times 10^{-3}$ g cm^2 is the measured moment of inertia around the vertical axis of the fly (*Musca domestica*) and $k \simeq 0{\cdot}18$ g cm^2 sec^{-1} represents an aerodynamic friction constant. Interestingly, $\Theta/k \simeq 8 \times 10^{-3}$ sec is very small, implying that the angular speed is always essentially proportional to the instantaneous torque; in other words the asymptotic situation $-\dot{\psi}$ proportional to F – is almost immediately reached (the time constant is $\Theta/k \simeq 8 \times 10^{-3}$ sec). $F(t)$, the instantaneous torque of the fly, is assumed to depend on the error angle function $\psi(t)$ (see section 3.3). Equation (2.1) can be rewritten in terms of the error angle as

$$\Theta\ddot{\psi}(t) + k\dot{\psi}(t) - \Theta\ddot{\alpha}_p(t) - k\dot{\alpha}_p(t) = -F\{\psi(t), t\} \tag{2.2}$$

or

$$\Theta\ddot{\psi}(t) + k\dot{\psi}(t) = -F\{\psi(t), t\} + S(t), \tag{2.3}$$

with

$$S(t) = \Theta\ddot{\alpha}_p(t) + k\dot{\alpha}_p(t).$$

When $\alpha_p(t) \equiv 0$, that is the object does not move with respect to the environment and $S(t) \equiv 0$, $\psi(t) \equiv -\alpha_f$. Equation (2.3) describes the free

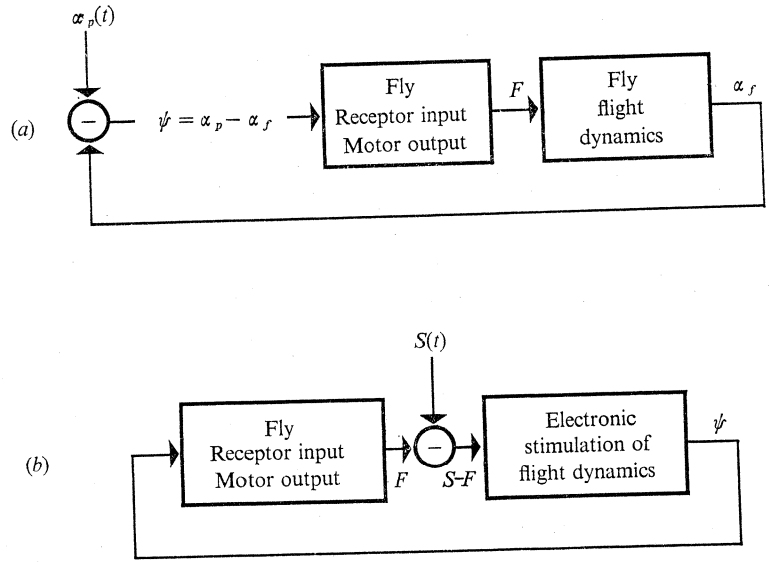

Fig. 2. (*a*) Signal flow diagram referring to the free flight situation of Fig. 1. The fly's transduction of the visual input into angular displacement can be split into two 'boxes'. The visual-input torque-output 'black-box' is followed by a 'box' representing the flight dynamics, transducing torque into angular displacement. (*b*) Signal flow diagram of the flight simulation device. The flight dynamics is simulated by analogue electronics. $S(t) = \Theta\ddot{\alpha}_p(t) + k\dot{\alpha}_p(t)$ simulates the object motion.

flight situation *in the coordinate system* of the fly. The equivalent 'closed-loop' signal flow diagram is shown in Fig. 2(*b*). A method to simulate the free flight conditions represented by equation (2.3) is given by the set-up schematized in Fig. 3, and described in detail elsewhere (Reichardt & Wenking, 1969; Reichardt, 1973). Although the orientation behaviour of the fly can be studied also with other methods most of the experiments described in this paper have been performed with the method shown in Fig. 3 or modifications of it (Virsik, 1974; Virsik & Reichardt, 1974, 1976). The characteristic variable directly observed in these experiments is the 'error angle' $\psi(t)$: the 'closed-loop' situation simulated in the set-up of Fig. 3 takes place in the coordinate system of the fly. A reconstruction of the trajectory $\alpha_f(t)$ can be calculated from a knowledge of $\psi(t)$ and $\alpha_p(t)$. However, the interesting information about the process is more directly contained in $\psi(t)$, which gives the 'history' of stimulation of the eye.

A similar set-up was used to investigate the height orientation be-

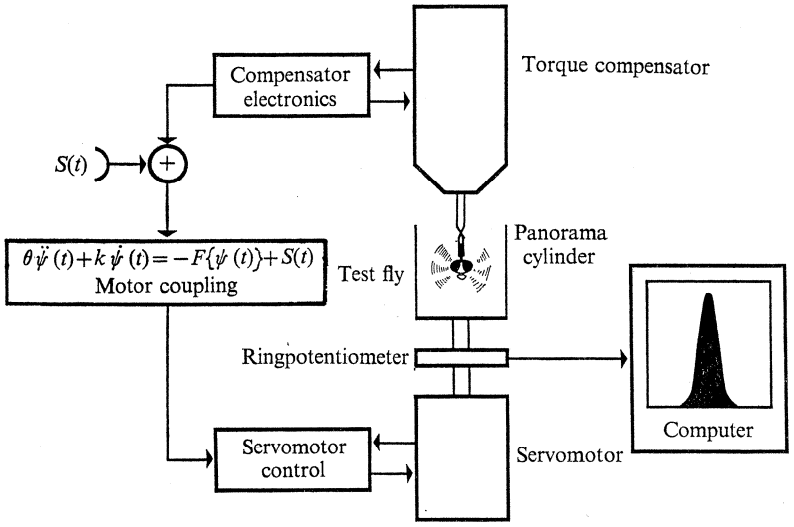

Fig. 3. Simplified scheme of the experimental set-up (closed-loop system). A fly, suspended from the torque compensator, controls the velocity of a cylindrical 'panorama' by its own torque signal. The transfer properties of the compensator, the motor coupling block and the servomotor approximate free flight dynamics (equation (2.1)). The instantaneous position of the panorama is signalled by a ringpotentiometer for further data processing. For more details, see text. Redrawn from Reichardt (1973).

haviour of flies (Wehrhahn, 1974; Wehrhahn & Reichardt, 1973, 1975). Corresponding to equation (2.3) a second-order differential equation in the vertical coordinate z (height) relates the lift of the fly to its vertical displacement. The equation reads

$$m\ddot{z}(t)+k_z\dot{z}(t) = P\{\theta(z(t)), t\}+L_0, \qquad (2.4)$$
$$\theta(z) = \arctan z/d,$$

where m is the fly's mass, k_z is a friction constant associated to this degree of freedom. The functional $P\{\theta(z(t)), t\}+L_0$ represents the fly's lift response to the object's vertical displacement z, at a distance d. The coordinate θ is the vertical angular error with respect to the equator of the fly's eye.

3. Phenomenological theory

In this section we describe an attempt to unravel the nature of the control system that enables a flying fly to fixate and track an object. A few key experiments will be described. Their results lead to the formulation of

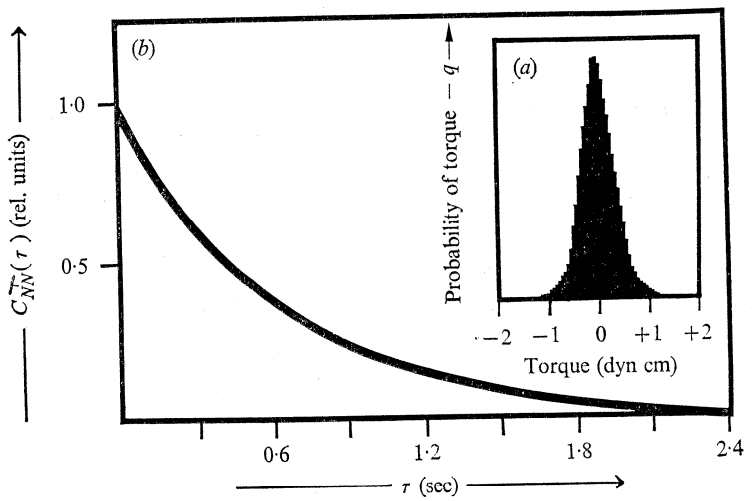

Fig. 4. The inset (*a*) shows a histogram of the torque fluctuation generated by a fly in a no-contrast, uniformly illuminated environment (open-loop experiment), during quiet, undisturbed flight. As shown by statistical tests, the histogram is, under these conditions, in good approximation gaussian. The random torque process leads, through the flight dynamics, to a flat asymptotic probability distribution of α_f. The normalized autocorrelation of the open-loop torque fluctuation is shown in (*b*). The autocorrelation is well described by the exponential $C_{NN}(\tau) = A\,e^{-\gamma\tau}$ with $\gamma = 1{\cdot}9$ [sec^{-1}] and $\sqrt{A} = 0{\cdot}3$ dyn cm ($\sqrt{A}$ is given by the standard deviation of the histogram (*a*)). Redrawn from Poggio & Reichardt (1973*a*).

a phenomenological theory of the fly's orientation behaviour, which can account for a variety of more complex situations.

3.1. *Spontaneous behaviour*

In a no-contrast homogeneously illuminated environment a fly flies in all directions α_f with equal probability. In fact, when these conditions are simulated in the experimental set-up of Fig. 3 the fly's torque turns out to be a stationary, zero-mean, stochastic signal $N(t)$ with a gaussian density distribution and an exponential autocorrelation

$$C_{NN}(\tau) = A\,e^{-\gamma\tau},$$

shown in Fig. 4(*a*) and (*b*). Under the assumption of gaussianity, the process $N(t)$ is completely and quantitatively characterized by its autocorrelation (Poggio & Reichardt, 1973*a*). In the limit $A \propto \gamma$, $\gamma \to \infty$ the $N(t)$ process would become a gaussian 'white' noise with a delta-peaked autocorrelation function. In this case $\alpha_f(t)$ would be a 'brownian motion'

process. Without visual contrast stimuli the fly spontaneously 'searches around', apparently in a random (but correlated) manner. Interestingly, a small, black object which does not move relative to the fly's retina does not affect the torque signal of the fly. Thus, stabilized retinal images of this kind do not apparently influence the orientation behaviour of the fly (see also Part II).

3.2. *Visually induced behaviour*

Visually induced behaviour occurs whenever a contrasted 'panorama' moves relative to the fly's retina. The most elementary type of orientation behaviour can be observed in the device shown in Fig. 3 when the cylindrical panorama contains a dark object in front of a white, illuminated background. Under closed-loop conditions the fly's instantaneous torque determines an angular displacement of the object relative to the retina according to equation (2.3). In the equivalent free flight situation flies orientate towards the black object either standing ($\alpha_p(t) = S(t) \equiv 0$) or moving ($\dot{\alpha}_p(t) \neq 0$; $S(t) \neq 0$), relative to the room coordinate system. In the first instance this orientation behaviour will be called 'fixation', in the second 'tracking'. In both cases a random *relative* motion between the object *and* the fly's retina occurs continuously, apparently provided by the continuous presence of the process $N(t)$. The histograms of Fig. 5 show the fraction of time the fly gazes at any part of the 'panorama' which carries a black vertical stripe. The histograms show clearly that during stationary fixation the fly's 'gaze' is directed in the mean towards the object ($\overline{\psi(t)} = 0$). Fixation of the stripe takes place irrespective of the initial position of the object on the fly's retina.

In summary, visual orientation is mediated, under natural conditions, by *relative* motion of a *contrasted* pattern with respect to the fly's retina. As will become clear in Part II *changes* of the light inputs to the receptors are the necessary prerequisites for the nervous computations underlying the visual control of flight. Under normal free flight conditions the critical stimulus for visual control of flight is the relative *movement* of *contours*. It is well known that flies, as other insects, show a direction sensitive optomotor response to relative movements of patterns. In other words a fly tries to turn in order to minimize the slip speed of a moving pattern. In addition, a direction insensitive optomotor response can be also elicited by small dark objects, like stripes. This response is position dependent: the fly tries to turn towards the object (Reichardt, 1973; Pick, 1974*a*). It is clear that this response component, together with the

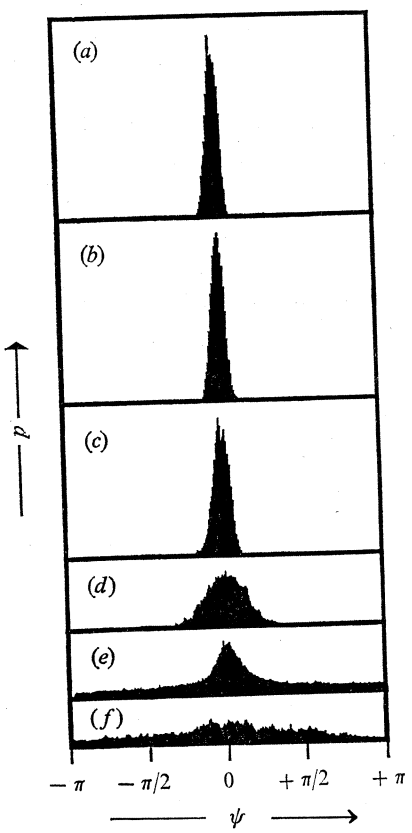

Fig. 5. Stationary (asymptotic) fixation of a 5° wide, vertically oriented black stripe. The histograms show the fraction of time the fly fixated any part of the panorama – that is, the fraction of time associated to any value of the error angle ψ. Parameter is the average brightness of the panorama from $1{\cdot}75 \times 10^{3}$ cd/m^2 (*a*) to $1{\cdot}21 \times 10^{-2}$ cd/m^2 (*f*) (lamps type: fluorescent ring bulbs Philips TLE 40 W/34 de Luxe). Decreasing light intensity degrades fixation until the ψ-distribution is in (*f*) almost flat. The light intensity used in most experiments described in this paper is the same given for Fig. 5(*a*). From Reichardt (1973).

natural symmetry of the two compound eyes, should play a critical role in object fixation under natural (closed-loop) conditions. The next section deals with a mathematical formulation of these observations.

3.3. *The phenomenological equation*

The observations described in the previous section suggest that the fly's torque underlying the orientation behaviour consists of two main components: a stationary, gaussian random process $N(t)$, essentially inde-

pendent from visual input *and* a visually induced response $R\{\psi(t), t\}$ regarded as a *functional* of $\psi(t)$, the error angle of the object on the retina of the fly. The simplest assumption consistent with the experimental results is that $N(t)$ and $R\{\psi(t), t\}$ add in the nervous system. Thus, the fly's torque can be written as

$$F\{\psi(t), t\} = N(t) + R\{\psi(t), t\} \tag{3.1}$$

and equation (2.3) becomes

$$\Theta\ddot{\psi}(t) + k\dot{\psi}(t) = N(t) - R\{\psi(t), t\} + S(t), \tag{3.2}$$

since the sign of the zero-mean random signal $N(t)$ does not matter.

The assumption contained in equation (3.1) can, at present, only be described as a first order approximation (Poggio & Reichardt, 1973 *a*). It is, however, quantitatively consistent with all the experimental results, so far. In particular, a specific experiment directly supporting equation (3.1) will be described in the next section. Interestingly, very recent electrophysiological data support the validity of equation (3.1). Heide (1975) has studied the optomotor response of the fly *Musca domestica* at the level of the neural output which controls the activity of the flight muscles. Visually induced as well as spontaneous turning activities can be observed and both are performed by the same combination of muscles. The physiological data lead to a diagram of information flow from the CNS to the flight muscles. The point of interest to us is that visually dependent information and spontaneous yaw-turn neural commands are *separate*, independent inputs, *adding* at the level of the muscle motoneurons (or earlier). This physiological evidence means that our hypothesis, given in equation (3.1), may be essentially more than a convenient phenomenological description and that separate neural structures could correspond in the CNS to the two terms of equation (3.1). As we will briefly discuss later, this conclusion is by no means necessarily implied by equation (3.1) alone.

Let us now consider the term $R\{\psi(t), t\}$. The following assumption plays a critical role in the formulation of the phenomenological theory: the visually induced torque $R\{\psi(t), t\}$, at the instant t, is given by a functional of the past history of the object position. Parameters are light intensity, the pattern itself and other similar quantities. Three points are important. First, the visually induced response is independent of the visual motor loop being open or closed. It depends only on the 'history' of the error angle $\psi(t)$ up to the instant t. Secondly, the response of the fly is time invariant, under our experimental conditions, implying that

R does not explicitly depend on t. Thirdly, the value of $R\{\psi(t)\}$ at t is much more 'sensitive' to changes of ψ in the near past than to changes at instants far away from t. Under those conditions one expects that, if $\psi(t)$ does not change too quickly, the functional $R\{\psi(t)\}$ should be given approximately by a function R^* of the value of ψ and its first n derivatives at t

$$R\{\psi(t)\} \sim R^*(\psi(t), \dot{\psi}(t), \ddot{\psi}(t)\ldots). \tag{3·3}$$

Theorems which justify this expectation, under reasonable conditions, do in fact exist (Coleman, 1971*a*).

In the fly's case, under normal (natural) coupling conditions and when the object does not move too fast, the visually induced response involves indeed a shorter time scale than the error angle history $\psi(t)$. Equation (3.2) shows why: neglecting $N(t)$ and $S(t)$, $\psi(t)$ turns out to be a low-pass filtered version of R (with $\Theta \sim 0$ the solution $\psi(t)$ is $\psi(t) = (1/k)\int R\,dt$). Thus, a first order approximation of equation (3·3),

$$R\{\psi(t)\} \simeq D(\psi(t)) + r(\psi(t))\,\dot{\psi}(t), \tag{3·4}$$

should provide a good representation of the visually induced response, under normal conditions. However, it is clear that whenever $\psi(t)$ is not 'smooth' enough (for instance under stronger unnatural coupling conditions – large k – see Poggio & Reichardt, 1973*a*) equation (3.4) may break down. The mathematical justification for equation (3.4) can be made precise, together with the conditions under which it is valid.†

The important point here is that the validity of equation (3.4) has been in fact verified experimentally under a variety of conditions (Reichardt, 1973; Poggio & Reichardt, 1973*a*; Reichardt & Poggio, 1975; Virsik & Reichardt, 1976). It must be realized that the large range of validity of equation (3.4) is not trivial. It is an experimental fact of some significance. Even the dead time between visual input and motor response is very small – certainly less than 30 msec (Land & Collett, 1974; S. Buchner & Reichardt, 1976) and can be neglected in most of the cases we shall consider later. Thus, equation (3.2) can be rewritten as

$$\Theta\ddot{\psi}(t) + k\dot{\psi}(t) = N(t) - D(\psi(t)) - r(\psi(t))\,\dot{\psi}(t) + S(t) \tag{3·5}$$

with $$C_{NN}(\tau) = A\,e^{-\gamma\tau}.$$

The functions $D(\psi)$ and $r(\psi)$ depend on the particular pattern and on other parameters. In the special but important case of a narrow vertical

† For instance, $D(\psi)$ and $r(\psi)$ in general depend on the zero-order input function $\psi(t)$ (see Coleman, 1971*a*). This point is important in comparing various experimental situations.

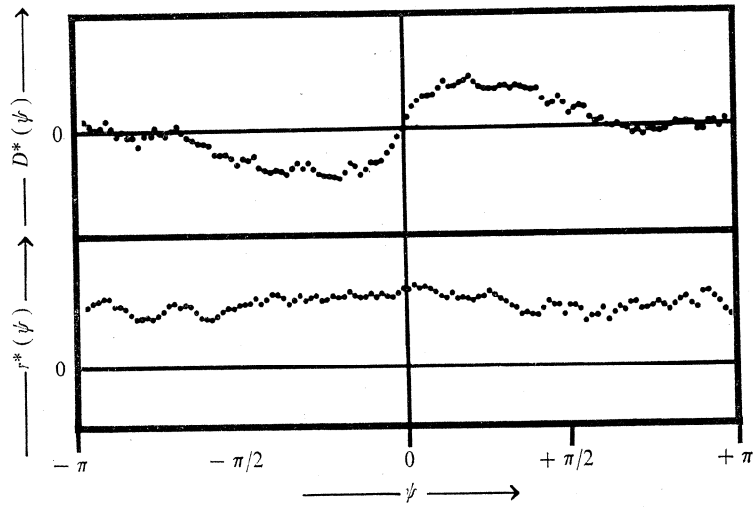

Fig. 6. The functions $D^*(\psi)$ and $r^*(\psi)$, in relative units, associated with the response of the fly (see equation (3.4)) to a narrow vertical black stripe segment (5° wide, 22·5° long). The stripe segment was rotated with a constant angular speed (8°/sec) and the measured (open-loop) torque was decomposed into the direction-insensitive component $D^*(\psi)$ and into the direction-sensitive one $r^*(\psi)\,\dot{\psi}$. The stripe segment was presented to the lower parts (below the equator) of the compound eyes. While $r^*(\psi)$ remains essentially unchanged, $D^*(\psi)$ is significantly smaller when the upper parts of the compound eyes are stimulated. The figure represents the average of five experiments, each one lasting about 6 min. From Poggio & Reichardt (1976).

black stripe (5° wide, 90° long) these functions, denoted as $D^*(\psi)$ and $r^*(\psi)$, have been measured with different methods, under the condition of $\psi(t)$ 'smooth' enough. Fig. 6 shows the $D^*(\psi)$ and $r^*(\psi)$ associated to a black vertical segment: the instantaneous open-loop response $R\{\psi(t)\}$ to the object rotating at small constant speed around the fly was measured for each ψ. Under the assumption that equation (3.4) holds, the two components $r^*(\psi)\dot{\psi}$ and $D^*(\psi)$ were identified through their respective symmetry properties (in $\dot{\psi}$). It will be sometimes convenient in the following to define a 'potential' function $U(\psi)$ through the formula†

$$D(\psi) = \partial U/\partial\psi. \tag{3.6}$$

Both $D^*(\psi)$ and $U^*(\psi)$ are shown in Fig. 7(*a*): in this case the experimental technique is different from the one used in the experiment shown in Fig. 6. Also other methods (Reichardt, 1973; Reichardt & Poggio, 1975)

† The definition of $D^*(\psi)$ used in this paper is slightly different (modulus the sign) from previous papers.

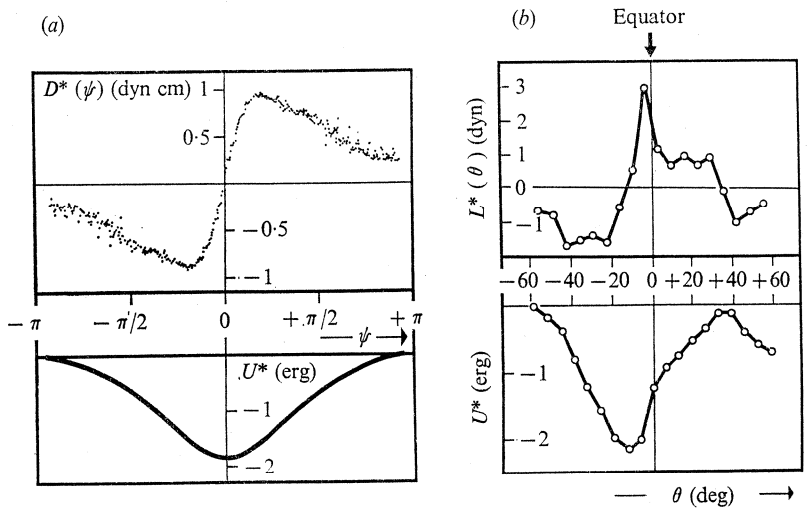

Fig. 7(*a*) The (direction-insensitive) torque response component $D^*(\psi)$ induced by a vertical black stripe (5° wide, $-45° \leqslant \theta \leqslant 45°$) and the associated 'potential' (lower diagram). Average from measurements on 111 flies. The function $D^*(\psi)$ represents the mean 'attractiveness' towards the stripe, for each ψ (see equation (3.4)). To avoid a 'stabilized retinal image', to which the fly would not respond, the stripe was randomly oscillated by the fly around each ψ position with small amplitude (partial closed-loop conditions, see Reichardt, 1973). The 'attractiveness' profile $D^*(\psi)$ does not significantly depend on the motion spectrum of the stripe (compare also Fig. 6 and Fig. 15) as long as the contrast changes at the level of the receptors are between 0·5 and 15 Hz. Redrawn from Reichardt (1973).

(*b*) The (direction-insensitive) response component $L^*(\theta)$, induced by a horizontally oriented black stripe, moved in the vertical (z) direction (upper diagram) and its corresponding potential (lower diagram), according to $L^*(\theta) = \partial U^*(\theta)/\partial\theta$. Average from measurements on seven flies. θ is the vertical angle between the equator, the optical symmetry line between upper and lower half of the eye, and the angular position of the stripe. Redrawn from Wehrhahn & Reichardt (1975).

provide consistent evaluations of the terms $D^*(\psi)$ and $r^*(\psi)$, as long as the conditions of validity of equation (3.4) are respected. In principle, tracking of a fast randomly moving target may not be well described by equation (3.5). However, in section (6.5) it will be shown that even under such extreme conditions the $D^*(\psi)$ function of Fig. 7(*a*) is a good approximation of the fly's response and that higher order terms are not strictly necessary.

The importance of $D^*(\psi)$ and $r^*(\psi)$ associated with an individual stripe derives from the fact that any small contrasted object will elicit a similar) response, apart from scaling factors. In section 7 we will show that the $D(\psi)$

and $r(\psi)$ associated to an arbitrary pattern can be well approximated from the functions of Fig. 7(*a*). In this sense the knowledge of $D^*(\psi)$ and $r^*(\psi)$ associated to a single stripe are basic to the phenomenological description of the orientation behaviour. An important question in this context concerns the 'vertical' parametrization of the functions D and r when small objects are used. To anticipate the results somewhat, it seems that the $r(\psi)$ term is homogeneously present all over the eye, while the term $D(\psi)$ is essentially present only in the lower part of the eye, below the equator.

$D^*(\psi)$ turns out to be an antisymmetric function, independent, to a first approximation, from the speed $\dot{\psi}$ (*at least* inside the range $2°/\text{sec} \leqslant \dot{\psi} \leqslant 50°/\text{sec}$). The coefficient $r^*(\psi)$ turns out to be well approximated by a constant r^*. Therefore, one term $(r^*\dot{\psi})$ is direction-sensitive, velocity-dependent *and* position-independent; the other term $(D^*(\psi))$ is direction-insensitive, velocity-independent *and* position-dependent. For a dark vertical stripe the visually induced response of the fly takes the form

$$R_{st}\{\psi(t)\} \approx D^*(\psi(t)) + r^*\dot{\psi}(t), \tag{3.7}$$

under the conditions mentioned before.

We have now reached the core of the formulation of the phenomenological equation describing the orientation behaviour. The visual control system the fly uses consists of two basic operations: one transduces *position* (angular error) into torque through the 'attractiveness' term $D(\psi)$; the other converts velocity into torque, through the term $r\dot{\psi}$. Thus, two basic computations are performed on the visual input. The first extracts *position* information $(D(\psi))$. The second gives *movement* information $(r\dot{\psi})$.

In Part II we will attempt to explain *how* these computations are performed in the visual system of the fly. The central thesis of this Part I is that these computations, characterized in terms of equation (3.4), lead, with the fluctuation process $N(t)$, through an approximation of the flight dynamics, to a phenomenological equation which can account for fixation, tracking and eventually spontaneous pattern preference behaviour. The equation in the error angle reads, for a black vertical stripe,

$$\Theta\ddot{\psi} + k\dot{\psi} + r^*\dot{\psi} + D^*(\psi) = N(t) + S(t), \tag{3.8}$$

where ψ (and $D^*(\psi)$) are modulus 2π. Therefore, the (natural) closed-loop behaviour can be predicted from the knowledge of open-loop responses. In this sense the phenomenological theory provides the critical

link between the (open-loop) studies on visual information processing in the fly's nervous system, either behavioural or electrophysiological, and the behaviour in natural conditions. Whether the artificial closed-loop conditions described in this paper are indeed representative of the free flight situations, will be discussed in section 6.6.

It is worth while to remark that one may take into account in equation (3.8) the dead time ϵ involved in the fly's torque response. However, for the fixation and the tracking situations described in *this* paper the delay actually involved ($\epsilon < 30$ msec) can be neglected.

An equation similar to equation (3.8) can be derived in an essentially equivalent way for the height orientation behaviour, whose dynamics was described by equation (2.4). The equation for a horizontally oriented black stripe is

$$m\ddot{z}+k_z\dot{z}+r^*_\theta\dot{\theta}(z)+L^*(\theta(z))=N_\theta(t), \qquad (3.9)$$
$$\theta=\arctan z/d,$$

where $L^*(\theta)$ is shown in Fig. 7(*b*) and $r^*_\theta\dot{\theta}$ represents the direction-sensitive component of the optomotor response. $N_\theta(t)$ is a stochastic gaussian lift fluctuation: its quantitative characterization has been given by Wehrhahn & Reichardt (1975). The structure of equations (3.8) and (3.9) is well known. They are nonlinear stochastic differential equations called in physics Langevin equations. For $S(t)=0$ they describe the motion of a representative point (ψ or θ) in a potential well ($U^*(\psi)$ or $U^*(\theta)$), under the effect of a random force (N or N_θ), in presence of friction (r^*+k or $r_\theta+k_z$). Thus, the *form* of the phenomenological equations leads to a straightforward analogy between the orientation process and the quasi-brownian motion of a particle in a potential well. In the case of equation (3.8) the minimum of the potential well at $\psi=0$ gives the most probable direction of gaze, in other words the maximum in the fixation histograms (if $S(t)\equiv 0$); the error angle $\psi(t)$ fluctuates around $\psi=0$, which is the stable equilibrium point of the process. Clearly, if the noise term $N(t)$ would be identically zero, the resulting deterministic equation would have, with $D^*(\psi)$ of Fig. 7(*a*), the trivial asymptotic solution $\psi(t)=0$. Since, however, the noise term actually exists, we are confronted with the problem of 'solving' a stochastic non-linear differential equation under various conditions of fixation and tracking. Of course, taking expected values of the various terms of equation (3.8) one obtains an ordinary differential equation in the expected value $\langle\psi(t)\rangle$. In some cases this is a satisfactory characterization of the orientation process, especially for fast tracking situations,

when $N(t)$ is small compared to $S(t)$. In similar cases the fly's eigenbehaviour arising from $N(t)$ may be masked by the experimental errors (compare Land & Collett, 1974). However, a faithful description of tracking and fixation has to take into account its essentially stochastic nature. Before digressing to the mathematics of the orientation behaviour we will present some experimental evidence supporting the phenomenological description derived in this section and we will introduce a simple linear approach to the fixation behaviour.

4. Simple applications of the theory

4.1. *A linear approach*

The shape of the term $D^*(\psi)$ implies that, under our coupling conditions, equation (3.8) can be linearized if the fluctuations of $\psi(t)$ are restricted to the linear range of $D^*(\psi)$. To check this requirement of the theory a simple tracking experiment has been performed. The experiment is a critical test for the general structure of equation (3.8) and some of its underlying assumptions (like the decomposition of equation (3.1)).

In the set-up shown in Fig. 3 artificial gaussian 'noise' was injected at the output of the torque compensator. In terms of equation (3.8) this simply means that the term $S(t)$ was chosen as a gaussian process $[S(t) = N_i(t)]$, independent from the $N(t)$ fluctuation produced by the fly. The experiment simulated a free flight situation in which the fly tracks a black vertical stripe moving with an angular velocity $\alpha_p(t)$ proportional to $N_i(t)$, relative to a fixed coordinate system. In the linear range of equation (3.8) ($-30° \leqslant \psi \leqslant 30°$) one thus expects that the increase in the mean square error angle $\langle[\psi(t)]^2\rangle = \sigma^2$ should be proportional to the mean square amplitude of the process $N_i(t)$ (Poggio & Reichardt, 1973*a*). Fig. 8 shows that the expectation is very precisely confirmed by the experimental data. An analogous result also holds for the height orientation behaviour (Wehrhahn & Reichardt, 1973, 1975). The result supports

(*a*) the decomposition of the fly's torque into a stochastic term $N(t)$, independent from $\{\psi(t)\}$, and a visually induced response $R\{\psi(t)\}$,

(*b*) the assumption that the response $R\{\psi(t)\}$ only depends on the error angle $\{\psi(t)\}$,

(*c*) the possibility to linearize equation (3.8) for $-30° \leqslant \psi \leqslant 30°$. It is worth while to mention that linearity is also suggested by the gaussianity of the closed-loop fluctuations in the experiment of Fig. 5(*a*, *b*, *c*) (see

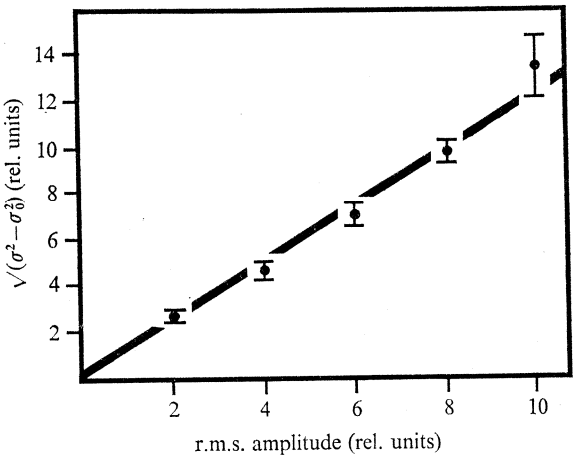

Fig. 8. Experimental relationship between the standard deviation σ of a fixation histogram and the power (in arbitrary units) of an artificial gaussian noise $N_i(\psi)$ injected additively into the closed loop. σ_0 represents the standard deviation of the fixation histogram without artificial noise. The points are averages taken from five flies. The artificial gaussian noise used in this experiment had a flat spectrum up to 15 Hz. The equivalent free flight situation corresponds to tracking by the fly of an object moving with an angular speed $\dot{\alpha}_p(t)$ proportional to the artificial noise: $\dot{\alpha}_p(t) = [N_i(t)]/k$. The ordinate of the figure indicates how the r.m.s. of the 'error angle' ψ_{tr} increases with increasing r.m.s. of the object's velocity. From Poggio & Reichardt (1973*a*).

also Fig. 9(*b*). It is well known that the characteristic variables of a closed-loop system are gaussian for gaussian input processes, *if* the system dynamics is linear.

4.2. *Fixation*

In the range $-30° \leqslant \psi \leqslant 30°$ equation (3.8) takes the linear form

$$\Theta\ddot{\psi} + k\dot{\psi} + r^*\psi + \beta\psi = N(t) + S(t) \qquad (4.1)$$

with $$C_{NN}(\tau) = A\,\mathrm{e}^{-\gamma\tau},$$

where the coefficient β represents the slope of the $D^*(\psi)$ characteristics around $\psi = 0$ (see Fig. 7*a*). For $S(t) = 0$ equation (4.1) is a linear stochastic equation in the 'error angle' $\psi(t)$. In this case standard methods of solution (see Wax, 1954; Martin, 1968) are available. Since $N(t)$ is a gaussian random process, completely defined by its auto-correlation, $\psi(t)$ must also be a gaussian random process. The stationary

solution is therefore simply given by the asymptotic probability distribution

$$p(\psi) = \sqrt{\left(\frac{1}{2\pi\sigma^2}\right)} \exp(-\psi^2/2\sigma^2). \tag{4.2}$$

The standard deviation σ can be easily obtained as

$$\sigma^2 = \frac{A}{\beta(k+r)} \frac{k+r^*+\gamma\Theta}{\beta+(k+r^*)\gamma+\gamma^2\Theta}. \tag{4.3}$$

Knowledge of the autocorrelation $C_{NN}(\tau)$ of the process $\psi(t)$ (Poggio & Reichardt, 1973*a*) can characterize completely the statistics of the random process $\psi(t)$, in terms of the various conditional probability distributions. However, equations (4.2) and (4.3) already show the role played by the various parameters. It is instructive to consider two approximations of equation (4.3). For $\Theta \to 0$ one obtains

$$\sigma^2 = \frac{A}{\beta(\beta+(k+r^*)\gamma)}. \tag{4.4}$$

In the 'white' noise limit ($A = c\gamma, \gamma \to \infty$), equation (4.4) becomes

$$\sigma^2 = \frac{c}{\beta(k+r^*)}, \tag{4.5}$$

with c being the spectral density of the white noise. While equation (4.4) is a good approximation, since Θ is actually very small, the assumption of $N(t)$ being white noise is certainly wrong. A comparison of the two equations shows the effect of the actually 'coloured' fluctuation process in determining the standard deviation of the error angle $\psi(t)$. More striking effects will be discussed later. The dependence on the fluctuation power is, of course, not surprising. The parameter β plays the main role: while an increase in either β or r^* leads to a 'better' stationary fixation (smaller σ), $\beta > 0$ is a necessary and sufficient condition for fixation. In terms of the brownian motion analogy the different roles of potential and friction are quite clear. In terms of standard feedback language the fly is equivalent to a position and a velocity servomechanism: fixation cannot take place without position sensitive information. However, speed-sensitive feedback can 'improve' stationary fixation. The linear equation (4.1) quantitatively predicts the stationary distribution of the process $\psi(t)$ for (normal) 'low' (Θ/k) couplings as Fig. 9 shows. The linear equation describes well also some tracking situations (Virsik & Reichardt, 1974, 1976) which, however, can be treated more completely in terms of the nonlinear equation (3.8) (see section 6). A very important

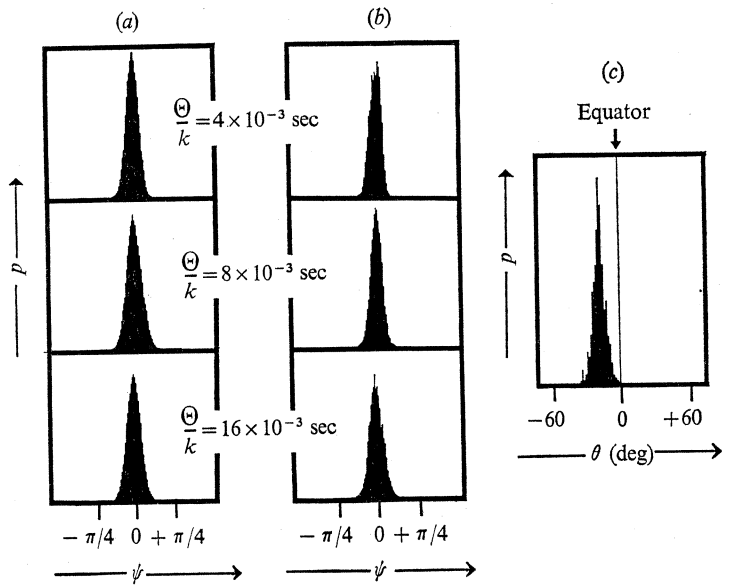

Fig. 9. Theoretical (*a*) and experimental (*b*) histograms of the error angle ψ, representing stationary fixation of a black, vertical stripe for different Θ/k values (normal, natural values are between $\Theta/k = 4\times10^{-3}$ msec and $\Theta/k = 8\times10^{-3}$ msec, with $\Theta = 1{\cdot}5\times10^{-3}$ g cm^2). The theoretical histograms have been obtained from equation (4.3); the values of the various parameters are derived from Figs. 4 and 7(*a*). The value of the parameter r^* has been determined through best fitting of one of the histograms shown here (for $\Theta/k = 4\times10^{-3}$). The histogram in (*c*) shows that a fly fixates a horizontal stripe, around a position $\theta \simeq -15°$, below the equator. This result indicates the existence of a 'functional fovea', in the lower part of the eye. Histograms like the one shown in Fig. 9(*c*) are well described by the equation in θ corresponding to equation (4.3) (see Wehrhahn & Reichardt, 1975). (*a*) and (*b*) redrawn from Poggio & Reichardt (1973*a*), (*c*) from Wehrhahn & Reichardt (1975).

point is that dynamic solutions in the expected value $\langle\psi(t)\rangle$, given by equation (4.1), agree with experimental results. A good example is provided by the chasing behaviour of *Fannia* (Land & Collett, 1974), for which a linear equation of the type of equation (4.1) holds in the larger range $-100° < \psi < +100°$ (equation (3) of Land & Collett coincides with our equation (4.1)).

4.3. *Role of movement- and position-dependent responses*

An interesting illustration of the effects of position and movement computation (the terms $\beta\psi$ and $r^*\psi$, respectively) is given by the sequence of experiments shown in Fig. 10. Necessary for a quantitative description

in terms of the phenomenological equation are the following three experimental facts:

(1) The visual 'noise' of the patterns shown in Fig. 10(b, c, d) elicits only a movement response ($r\dot{\psi}$), but no position response $D(\psi)$. This experimental fact is to be expected in view of the statistical isotropy of the pattern.

(2) The r parameter associated to each pattern is roughly proportional to the stimulated area of the eye (see Götz, 1964; McCann & MacGinitie, 1965).

(3) When the stripe segment is *embedded* in a 'noisy' texture (e.g. Fig. 10c, d), the associated attractiveness $D^*(\psi)$ is 'inhibited' by the noise. This masking effect, due to nonlinear lateral inhibitory interactions affecting the position computation (see Part II), is clearly to be expected on simple (even psychophysical) grounds. Experiments (Virsik, 1974) indicate that the slope of $D^*(\psi)$ of a black stripe embedded in a contrasted 'background' decreases as the contrast of the background increases from 0% to 100%.

It is now easy to interpret the experimental results in terms for instance of equation (4.3). The noise pattern in the upper half (Fig. 10b) of the panorama strongly increases r without affecting β: the 'friction' is increased and σ decreases. In Fig. 10(c) the noise pattern, while providing the same $r\dot{\psi}$ contribution, masks the stripe, thereby reducing β. In Fig. 10(d) β has the same value as in Fig. 10(c), but r is roughly twice as large, again reducing σ. The theoretical prediction of the outcome of the experiments rely on the nonlinear equation (3.8) and is in good *quantitative* agreement with the experimental data (Poggio & Reichardt, 1973*a*). Not only the stationary distributions are different in the four cases of Fig. 10, but also the dynamics of the process depends on the different values of r and β. It is easy to see from the autocorrelation that the time constant of the $\psi(t)$ process is slowed down by an increase in the friction r. The insets a' and b' in Fig. 10 show that this is clearly the case. The velocity term ($r\dot{\psi}$) 'stabilizes' the fixation process.

From this rather strong example, we see that the phenomenological description, derived in section 3.3, can account for the fly's orientation behaviour in non-trivial situations. The central role of movement *and* position information – the terms $r\dot{\psi}$ and $D(\psi)$ – in determining the orientation behaviour, emerges clearly from this last experiment. The spontaneous orientation of the fly towards a structured pattern can be predicted by the theory and, while simple, is not trivial, as Fig. 10 suggests.

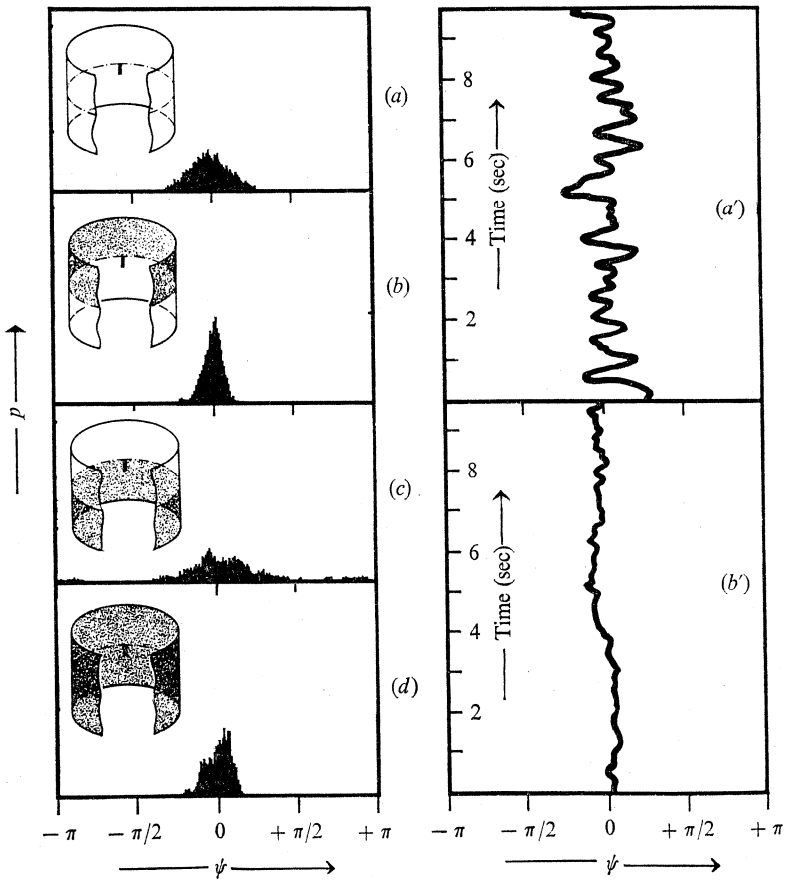

Fig. 10. Four different patterns (*a*, *b*, *c*, *d*) and the corresponding stationary orientation behaviours, represented in the lower parts of the figure through histograms of the error angle ψ. The rather different orientation behaviour elicited by the four patterns (contrast of the visual noise 50%) can be quantitatively predicted by equation (3.8) (Poggio & Reichardt, 1973*a*). The interplay of the movement and the position response associated to the four patterns (the terms $r\dot{\psi}$ and $D(\psi)$, respectively) determines the stationary orientation behaviour (left figures) and the dynamics of the fixation process (right figures). An increased value of the direction-sensitive optomotor response associated to the more structured pattern (*b*) significantly slows down (see Fig. *b'*) the fixation process $\psi(t)$ (and the corresponding fly's trajectory $\alpha_f(t)$) compared to pattern (*a*) (see Fig. *a'*). Left side of figure redrawn from Reichardt (1973).

Existing theories of spontaneous pattern preference in insects, based on figure parameters like contrast, area and contour, cannot account for the behaviour shown in Fig. 10. It is perhaps worth while to stress that while

the position control term $D(\psi)$ is critical for fixation and tracking, the error velocity term also plays, in general, an important role. First, it increases the stability of the process, e.g. allowing larger delays in equation (3.8), without causing instability phenomena, as Bode diagrams show. Secondly, the fly is able to track better since movement information in addition to position information helps to minimize the error angle. This is well known in the field of optimum tracking, where error terms containing speed, acceleration and eventually higher derivatives of the error angle may considerably improve the performance of a simple position controlled system (James, Nichols & Phillips, 1947). The interplay of 'friction' and 'potential', of a velocity and a position control, of direction-sensitive and direction-insensitive optomotor response, is also critical in various instances of tracking. Before approaching these cases, we need a better understanding of the nonlinear equation (3.8). In the next section we shall outline the relevant mathematics.

5. The mathematics of the theory

As we have mentioned earlier, equations of the type

$$\Theta\ddot{\psi}+[k+r(\psi)]\dot{\psi}+\frac{\partial U(\psi)}{\partial\psi}=N(t)+S(t), \tag{5.1}$$

with $$U(\psi)=U(\psi+2\pi n)\quad(n=0,1,\ldots),$$

where $N(t)$ is a 'physical' noise process, are known in physics as Langevin equations. In mathematics, they are usually interpreted either as Stratonovitch or Ito stochastic differential equations.† We follow here the physical notation and approach.‡ To solve the stochastic equation (5.1) is equivalent to characterize completely the statistics of the random process $\psi(t)$. When the equation is nonlinear, an exact solution is formally possible on the basis of the theory of Markov processes (Stratonovitch, 1968; Skorokhod, 1965). The statistics of $\psi(t)$ can be given by the Fokker–Planck technique which associates with equation (5.1) a partial differential equation in the instantaneous probability density of ψ. In this section we briefly outline some results important for the phenomenological description of the orientation behaviour. The derivation of the solutions is treated in more detail by Poggio & Reichardt (1973*a*) and Reichardt & Poggio (1975).

† Relations between the two approaches, the Langevin and the Ito approach, are discussed for instance by Wong & Zakai (1965) and Stratonovitch (1968).

‡ The proper stochastic analogue of the Langevin equation is here the Stratonovitch differential equation.

A preliminary point seems relevant here. The solution of equation (5.1) in terms of probability distributions of ψ instead of in terms of trajectories of $\psi(t)$ is dictated by the stochastic nature of the problem. Moreover, the comparison of stationary solutions of equation (5.1) with the stationary state of fixation and tracking behaviour is as significant as the comparison of transients. In other words the stationary solutions which we will derive here and the corresponding experimental data, characterize equation (5.1) and in turn its dynamic behaviour. To simplify here the treatment somewhat, we make the assumption that Θ is negligible, since its value is (in *Musca*) very small. Moreover, we assume that the friction parameter associated to a given pattern is a constant, independent from ψ: $r(\psi) = r$. At first we consider the 'fixation' case, corresponding to $S(t) \equiv 0$. If the random process $N(t) = W(t)$ were gaussian and white, $\psi(t)$ would then be a Markov process defined by

$$\dot{\psi} + \frac{1}{k+r}\frac{\partial U(\psi)}{\partial \psi} = \frac{W(t)}{k+r}, \tag{5.2}$$

where $W(t)$ would be white noise with a spectral density equal to c. In the more realistic case of $N(t)$ being a 'coloured' gaussian process with the first order autocorrelation shown in Fig. 4, equation (5.1), written in the phase space, takes the form

$$\dot{\psi} + \frac{1}{k+r}\frac{\partial U(\psi)}{\partial \psi} = \frac{N(t)}{k+r}, \tag{5.3}$$

$$\dot{N} + \gamma N = W(t),$$

where W is a gaussian 'white' noise process with spectral density $(A\gamma)$. The dynamical trajectory $[\psi, N]$ is a two-dimensional Markov process of which $[\psi]$ is a projection.

While a Fokker–Planck equation can be easily derived for equation (5.2) as well as for equation (5.3), its stationary solution, simple in the 'white' noise case, becomes rather complex in the realistic case of equation (5.3). For explanatory purposes we shall, at first, briefly consider the white noise case equation (5.2). The associated analytic solutions are illustrative of the qualitative features of the problem. Moreover, the 'white' noise assumption describes well fixation of patterns whose associated potential is 'small' compared to the associated friction, r, as in the case of large structured panoramas (see Fig. 10*b*, *c*, *d*).

The Fokker–Planck equation in the transition probability distribution

function $p(\psi; t)$ associated to equation (5.2) is

$$\frac{\partial}{\partial t}p(\psi; t) = \frac{\partial}{\partial \psi}\left[\frac{1}{k+r}\frac{\partial U(\psi)}{\partial \psi}p(\psi; t)\right] + \frac{c}{(k+r)^2}\frac{\partial^2}{\partial \psi^2}p(\psi; t). \quad (5.4)$$

Its stationary solution (for $t \to \infty$) can be easily derived from equation (5.4) and the appropriate boundary conditions† as

$$p(\psi) = C \exp\left(-U(\psi)\,(k+r)/c\right). \quad (5.5)$$

It relates an arbitrary nonlinear (cyclic!) potential $U(\psi)$, associated to a given pattern, to the stationary 'error angle' distribution $p(\psi)$. Therefore, once position and movement response ($D(\psi)$ and $r\dot{\psi}$) associated to a pattern are known, the spontaneous orientation behaviour of the fly is characterized in its stationary (or asymptotic) state by the stationary solution of the Fokker–Planck equation.

Interestingly, the mapping defined by equation (5.5) is a one-to-one correspondence between potential profile and $p(\psi)$. A large value of c (spectral density of the fluctuation process) maps the whole potential profile with equal weight. Small values of c, however, result in a mapping of practically only the minima of $U(\psi)$ into $p(\psi)$. As we shall see later, the potential of two or more objects show 'symmetry breakings' with respect to the potential minima. Concepts like phase transitions can be applied in these cases to the fly's pattern discrimination behaviour (Poggio & Reichardt, 1973*a*). These considerations, valid under the 'white' noise hypothesis, essentially apply also to equation (5.3). Since equation (5.3) and the associated Fokker–Planck equations do not satisfy the condition of detailed balance (Graham & Haken, 1971), no general method is available to obtain the stationary distribution. An approximate solution (Reichardt & Poggio, 1975), although not accurate for our normal parameter values, nevertheless fully illustrates the role played by the coloured spectrum. The approximate solution reads

$$p(\psi) \propto \exp\left\{-\frac{\gamma}{A}(k+r)\,U(\psi) - \frac{1}{2A}[D(\psi)]^2 + \frac{1}{\gamma(k+r)}\frac{\mathrm{d}D(\psi)}{\mathrm{d}\psi}\right\}, \quad (5.6)$$

and clearly shows that $p(\psi)$ *may* present two maxima, even if $U(\psi)$ has only one minimum. Due to the non-white spectrum of the fluctuations an 'early symmetry breaking' in the peaks of the probability distribution

† Since we are interested in $p(\psi; t)$, where ψ is taken modulus 2π, care must be used to define properly the desired distribution function (see for instance Lindsey, 1972).

can take place *without* a corresponding symmetry breaking in the potential minima. The effect illustrates the importance of the nature of the fluctuations, when not thermal-like, in determining the phase transition behaviour of a system (compare Nicolis & Prigogine, 1971). Section 6.4 will provide evidence that this is also the case for the fixation behaviour of the fly. However, in the majority of the situations equation (5·3) provides a satisfactory description of the main features of the stationary orientation process.

Up to this point we have considered fixation of a stationary pattern ($S(t) = 0$ in equation (5·1)). The tracking case ($S(t) \neq 0$) represents, in general, a more difficult problem. However, quite often $N(t)$ is negligible, relative to $S(t)$. If $S(t) = \Theta\ddot{\alpha}_p + k\dot{\alpha}_p$ is a known function (see equation (2.3)), equation (5·1) becomes then an ordinary differential equation in the expected value $\langle\psi(t)\rangle$. If $S(t)$ is a random process it might be possible to solve the stochastic equation (5·1) by means of the Fokker–Planck method (Poggio & Reichardt, 1973*a*). In particular, if $S(t)$ is a 'white' gaussian process relative to which $N(t)$ can be neglected, the stationary distribution equation (5·5) gives the solution, with c now representing the spectral density of $S(t)$.

Another important tracking situation occurs when the target moves at constant angular speed $\dot{\alpha}_p$. In this case (for $\Theta = 0$)

$$S(t) = k\dot{\alpha}_p(t), \quad \dot{\alpha}_p = \text{const.} \tag{5·7}$$

Defining a new (non-cyclic) potential (see Fig. 11) by

$$\tilde{U}(\psi) = k\dot{\alpha}_p\psi - U(\psi), \tag{5·8}$$

the associated Fokker–Planck equation has the solution, under the hypothesis of a 'white' fluctuation process $N(t)$,

$$p(\psi) \propto \exp\left\{\frac{k+r}{c}\tilde{U}(\psi)\right\}\int_{\psi-2\pi}^{\psi}\exp\left\{-\frac{k+r}{c}\tilde{U}(\psi')\right\}d\psi'. \tag{5·9}$$

Equation (5·9) can be interpreted as the probability distribution of a brownian particle in the non-cyclic potential $\tilde{U}(\psi)$, shown in Fig. 11(*a*). Necessary condition for the tracking of a stripe is $k\dot{\alpha}_p < \max_\psi D^*(\psi)$. The average error angle $\langle\psi_{tr}\rangle$, which depends on the speed of the target, on r^* and on $D^*(\psi)$, implies that the fly tracks the stripe with a certain lag (see Fig. 11*a*, *b*). Fig. 11(*c*) shows an experimental and a theoretical histogram for the probability distribution of the error angle ψ_{tr}, when a stripe is lost repeatedly.

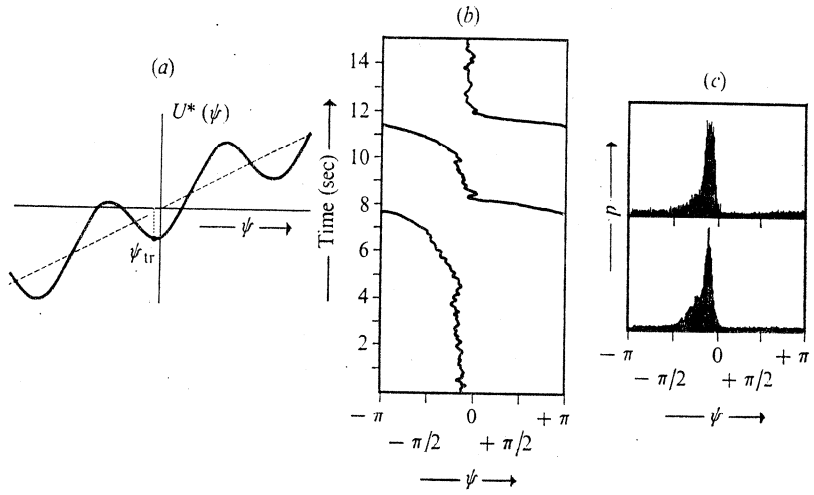

Fig. 11. (*a*) Tracking of a target moving at constant angular speed $\dot{\alpha}_p(t)$ is formally equivalent (through equation (5.9)) to the motion of a particle in a wavy inclined surface. In the absence of fluctuations (the spontaneous torque process $N(t)$) the representative point comes to rest at the bottom of one of the wells. Tracking is impossible if there are no 'bottoms' because of the excessive slope of the plane (the target's speed is too high). The fluctuation process dislodges now and then the representative point. Its average effect is to cause sliding of the point down the plane. Sliding (loss of tracking) occurs more rapidly the greater the slope (speed of the target), the shallower the wells (attractiveness of the target), the stronger the random excitations ($N(t)$).

(*b*) A typical trajectory of the error angle $\psi(t)$, modulus 2π, during tracking of a black vertical stripe moving at fast, constant angular speed $\dot{\alpha}_p$. The fly lags more and more behind the target, suddenly makes what appears as a sort of nystagmus, that is a fast turn against the direction of the target motion, locks again on the target and fixates for a while. Equation (5.9) and (*a*) clearly explain this behaviour, which has been also observed in walking *Tenebrio molitor* (Varjú, 1975) and in *Syritta pipiens*, hovering in a rotating drum (Collett & Land, 1975*a*).

The same fact is obvious in the histograms shown in Fig. 11(*c*). The upper histograms have been obtained through a digital simulation of equation (5.1) with $S(t) = k\dot{\alpha}_p$, $\dot{\alpha}_p$ = const. and standard values for the parameters, used throughout our paper. The lower histogram represents the result of a corresponding experiment. The fact that the peak of the distributions is shifted with respect to $\psi = 0$ means that the fly tracks the stripe with a certain mean angular lag ψ_{tr} (see also equations (6.1) and Fig. 12). (*c*) From Reichardt & Poggio (1975).

Various approaches can be used to characterize the statistics of the process $\psi(t)$ for different forms of equation (5.1). For instance, the probability of 'loss of target' can be evaluated in various ways. In our brownian motion analogy, loss of target under tracking or fixation corre-

sponds to the representative point 'jumping out' of a potential well. The problem belongs to the class of level-crossing problems for random processes. In previous papers we have derived approximate formulae giving the life-time of fixation or tracking (see equation (II. 20) in Reichardt & Poggio, 1975). The average time on target, which is a good measure of a tracking performance, can be thus evaluated and its dependence on the various parameters characterizing the pattern can be studied. A simple example of a situation which can thus be approached is shown in Fig. 11. A more complex experimental paradigm will be described in chapter 6.

The height orientation behaviour can be also described with the same mathematical technique. The only non-trivial mathematical difference is that the coordinate z and the associated functions [like the 'attractiveness' function $L^*(\theta(z))$] are not cyclic. Also in this case the Fokker–Planck method can characterize completely the statistics of the process $\theta(t)$. It is worth while to mention that the *horizontal* orientation behaviour of the fly, as described by equation (5.1), is formally equivalent to that of a coherent tracking loop (Lindsey, 1972). The analogy suggests various useful mathematical techniques; it may embed a much deeper meaning, pointing out general mechanisms which may underlie the orientation behaviour in insects.

The formalism outlined here can be easily extended to account for other more complex orientation situations. For instance, a complete description of body and head movements may be obtained modifying equation (5.1) as suggested previously (Poggio, 1972). Saccadic-like movements of the head may be described by Poisson-like terms; the underlying dynamics is still an open problem. Other extensions of equation (5.1), including for instance translatory movements of parts of the 'panorama' or additional degrees of freedom, may show a rich dynamical behaviour, perhaps providing other instances of the phase transition concept suggested earlier. A stability analysis of object tracking with lateral translations with respect to an environment can be easily carried out, applying a more recent approach of Götz (1975*a*) to the closed-loop stability of the direction-sensitive optomotor response.

In summary then, the analysis outlined in this section shows how the position dependent and the velocity dependent components of the optomotor response, together with the fluctuation $N(t)$, determine the (closed-loop) orientation behaviour. Our main thesis here is that, if $D(\psi)$ and (ψ) associated to a given pattern are known, the problem of characterizing (head-fixed) orientation and tracking is reduced to the mathematical

problem of solving the phenomenological equation. In the next section we will provide experimental evidence of the descriptive and predictive power of the basic equation (5.1).

6. Description of tracking and orientation

Orientation and tracking behaviour of the fly can be accurately predicted by the phenomenological theory in a number of experiments which have been performed so far. In this section we review some of the results. Other examples can be found in the literature (Reichardt, 1973; Poggio & Reichardt, 1973*a*; Reichardt & Poggio, 1975; Wehrhahn & Reichardt, 1975; Virsik & Reichardt, 1976; Land & Collett, 1974;† Varjú, 1975).

6.1. *Tracking of a target moving with constant angular velocity*

The analysis of this case has been outlined in the previous chapter. In equation (5.1) the terms $S(t)$ takes the form $S(t) = k\dot{\alpha}_p$, where $\dot{\alpha}_p$ designates the constant angular speed of the stripe. Characteristic conditions for stationary tracking are $\langle\ddot{\psi}\rangle = 0$, $\langle\dot{\psi}\rangle = 0$, which imply that the expected value of the error angle ψ is, through equation (5.1),

$$\langle\psi_{\mathrm{tr}}\rangle = \frac{k}{\beta}\dot{\alpha}_p, \tag{6.1}$$

where β is the slope of the linear part of $D^*(\psi)$ around $\psi = 0$. In other words, the fly lags behind the object by an average angle $\langle\psi_{\mathrm{tr}}\rangle$, which is proportional to the speed of the pattern (and inversely proportional to the slope β of the linear part of its 'attractiveness' function $D^*(\psi)$). For a black vertical stripe the maximum speed $\dot{\alpha}_p$ for which tracking can occur can be inferred from Fig. 7(*a*) to be around 300°/sec, corresponding to a maximum lag of *about* 20°. For higher speeds the target is lost more and more often, until no tracking takes place. These predictions are confirmed by the experiment shown in Fig. 12. Thus, (female) *Musca* can effectively track *fast* moving targets. Observe that, in the situation described here, image stabilization is essentially due to the position control system ($D^*(\psi)$) and does not require slip-speed between the fly and the target. Note that as long as the target is not lost too often ($\langle\dot{\psi}\rangle \simeq 0$) the

† Although Land and Collett do not explicitly mention it, they use the phenomenological theory (equation (4.1)) to describe chasing of *Fannia* and tracking by *Syritta* (see their equation (3)). Their work shows that the phenomenological theory applies also to free flight conditions.

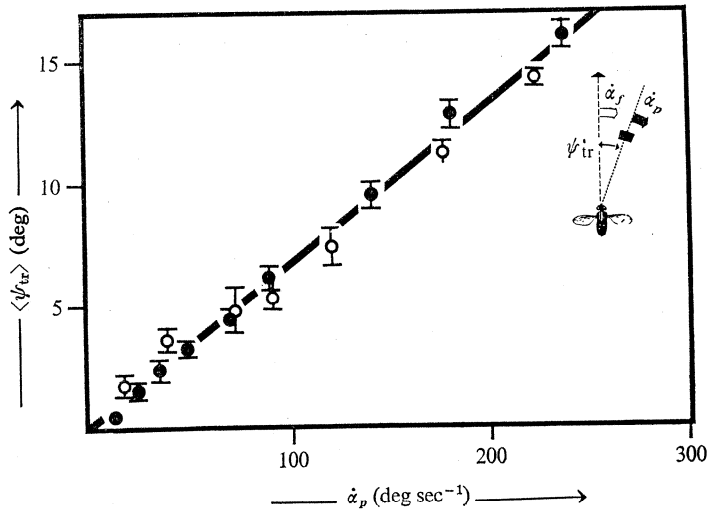

Fig. 12. The dependence of the tracking angle $\langle\psi_{tr}\rangle$ upon the constant angular velocity $\dot{\alpha}_p$ of a black stripe. $\langle\psi_{tr}\rangle$ designates the mean error angle between the flight direction and the position of the object. The inset shows the equivalent free flight condition: the fly tracks the object with the same average velocity ($\dot{\alpha}_p = \dot{\alpha}_f$) and an average error angle $\langle\psi_{tr}\rangle$. Every point in the diagram represents mean values from experiments with five different flies; the bars denote standard deviations of the means. The filled (open) circles correspond to measurements with flies having their heads fixed (free). Each measurement took 120 sec. The straight line represents the relation between $\langle\psi_{tr}\rangle$ and $\dot{\alpha}_p$ predicted by equation (6.1). Higher velocities of the stripe lead to increasingly frequent losses of tracking (see equation (5.9) and Fig. 11*c*). Redrawn from Visik & Reichardt (1976).

conditions under which equation (3.4) is valid ($\psi(t)$ 'smooth') still hold as in the fixation case ($\dot{\alpha}_p = 0$).

When $\dot{\alpha}_p$ is large and the target is lost again and again, the full equation (5.1) must be taken into account. Fokker–Planck techniques provide an evaluation of the probability of loss of target depending on the various parameters (see also Fig. 11 and Reichardt & Poggio, 1975). Target loss corresponds to an escape of the representative point from a potential well (see Fig. 11). The probability of target loss depends primarily on the 'height' of the potential barrier, on the curvature of the potential, on the friction and on the noise power and spectrum.

6.2. *Tracking of an object in front of a background*

If the target is embedded in a contrasted random-dot pattern and rigidly connected to it the description remains essentially the same (see equation (6.1)). The only difference is that the parameters r and β are here different

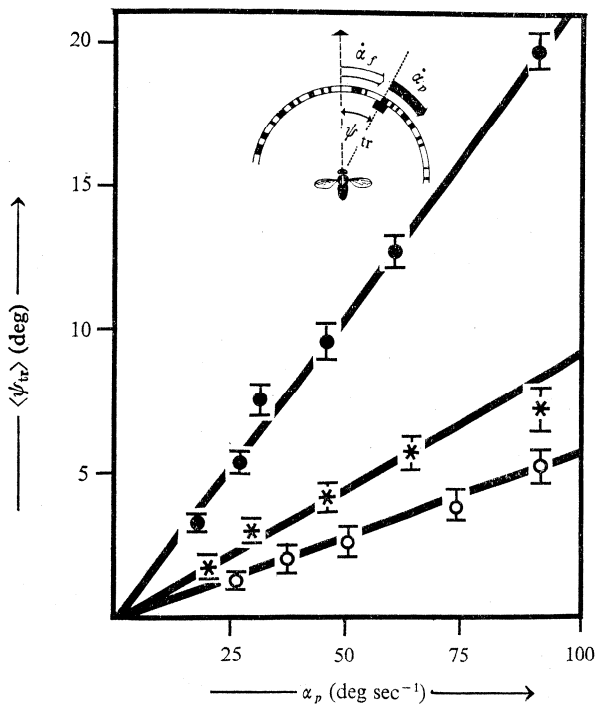

Fig. 13. Tracking of a black vertical stripe embedded in, and rigidly connected to, a contrasted random texture (all around). The fly (see inset) tracks the stripe, which moves at constant angular speed $\dot{\alpha}_p$, with the same angular speed $\dot{\alpha}_f = \dot{\alpha}_p$, and a mean angular lag $\langle\psi_{tr}\rangle$, which is shown here as a function of the object velocity. The contrast of the stripe was 100%; the contrast of the random texture was (m = 0% (○○○), m = 33% (***), m = 56% (●●●). Each point represents the mean value of five measurements (120 sec long) from five flies. Straight lines are regression lines; their slope can be also derived from equation (6.1). The slope (and the angular lag for given object's velocities) increases with increasing contrast of the background texture because the parameter β decreases: the stripe is increasingly masked by the background. The maximum speed for which tracking occurs without frequent losses (proportional to the maximum of $D^*(\psi)$) also decreases with increasing texture contrast (see section 6.1). Redrawn from Višik & Reichardt (1976).

since they depend on the contrast of the background texture, which 'masks' the object. Fig. 13 shows how the tracking angle increases with background contrast, since β decreases. For equal object and background contrasts $\beta = 0$: the object is not 'seen' by the fly. However, if 'incoherent' relative motion takes place between object and background texture, the 'masking' inhibition is destroyed (see Part II) and the parameter β, which is a measure of the attractiveness of the object, takes a

value characteristic of the no-texture situation. In Part II this appears as a consequence of the functional properties of the nervous interactions which compute the object attractiveness. The relevant point is that, at the phenomenological level of Part I, it is possible to describe tracking of an object moving at constant speed in front of a contrasted texture.

Equation (5.1) with $S(t) = k\dot{\alpha}_p(t)$ must now contain an additional term due to the fly's direction-sensitive optomotor reaction to the relative motion of the background texture. If expected values are taken, under the assumption that tracking occurs

$$(\langle\psi\rangle = \langle\psi_{tr}\rangle, \quad \langle\ddot{\psi}\rangle = \langle\dot{\psi}\rangle = 0),$$

it holds

$$\langle\psi_{tr}\rangle = \frac{k}{\beta}\left(1 + \frac{r_2}{k}\right)\dot{\alpha}_p, \tag{6.2}$$

where r_2 is associated to the direction-sensitive optomotor response elicited by the texture (Virsik & Reichardt, 1974). The fly and the object move with an average angular velocity $\dot{\alpha}_p$ with respect to the background pattern. Thus, $\langle\psi_{tr}\rangle$ and $\dot{\alpha}_p$ are proportional to one another as in equation (6.1) but with a larger proportionality factor. An interesting sideline to this is that if the coupling of the fly to the background is artificially inverted so that the background texture rotates in the same direction of the target with twice its average speed, equation (6.2) becomes

$$\langle\psi_{tr}\rangle = \frac{k}{\beta}\left(1 - \frac{r_2}{k}\right)\dot{\alpha}_p. \tag{6.3}$$

Equation (6.3) predicts that the tracking angle decreases and eventually changes its sign when $r_2/k > 1$. In this case, the angular *lag* during tracking becomes an angular *lead*. Equation (6.1) through equation (6.3) has been tested in a series of experiments for three different contrasts (r_2 increases with increasing contrast) of the background texture (Virsik & Reichardt, 1976). The experimental results are in complete agreement with the theoretical predictions. Fig. 14 shows the case in which the texture contrast is $m = 55\%$.

6.3. *Antifixation*

If, in equation (5.1), the sign of the fly's torque is artificially inverted one can simulate an extreme orientation situation, in which, for example, an attempt by the fly to turn to the right makes the panorama turn to the right, therefore simulating a turn to the left of the fly (Reichardt, 1973). The experiment provides a strong test of the validity of the phenomenological equation. In a sense it corresponds to an electronic interchange of

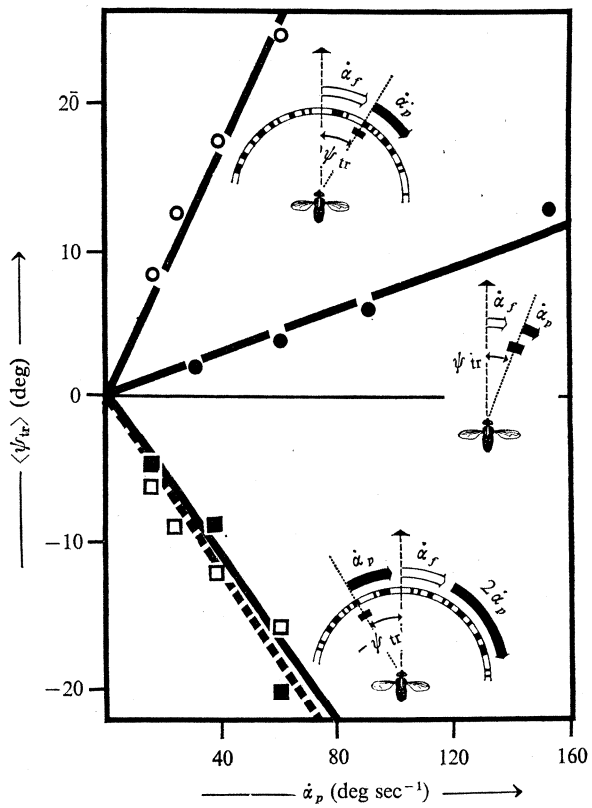

Fig. 14. Tracking of a black (100 % contrast) vertical stripe moving with constant angular speed $\dot{\alpha}_p$ in front of a background (360° around the fly). The fly tracks the stripe, which moves at constant angular velocity $\dot{\alpha}_p$, with the same angular velocity $\dot{\alpha}_f = \dot{\alpha}_p$ and a mean angular lag $\langle \psi_{tr} \rangle$, shown in the figure as a function of object velocity $\dot{\alpha}_p$. The mean values plotted here were obtained from one fly.

●●● = Tracking of the stripe in front of a white background. Corresponding to Fig. 12 (see insets) and equation (6.1).

○○○ = Tracking of the stripe in front of a random dot texture (360° angular extension) with an average contrast $m = 55\,\%$ (see equation (6.2)).

■■■ = Tracking of the stripe in front of the same random texture background but with reversed coupling of the fly to the background (see equation (6.3)).

□□□ = Predicted from the data ●●● and ○○○ by equations (6.1) through (6.3).

The full lines (the dotted line corresponds to the points □□□) are regression lines. Redrawn from Virsik & Reichardt (1976).

'left' and 'right' fly's motor outputs. The theory predicts (under the simplifying hypothesis of N being white) the following asymptotic distribution in ψ:

$$p(\psi) = C \exp\left\{\frac{k-r}{c} U(\psi)\right\}, \tag{6.4}$$

with the stability condition $(k-r) > 0$. Equation (6.4) should be compared with equation (5.5). When the pattern consists of a black vertical stripe, the associated $U^*(\psi)$, shown in Fig. 7(*a*), leads to an 'antifixation' of the stripe: the value $\psi = 0$, corresponding to a minimum of the 'potential' $U^*(\psi)$, is now unstable and the new stable error angle corresponding to the previous 'potential' maximum, is $\psi = \pm\pi$. The fly escapes from the stripe. Digital simulations of the corresponding equation, taking into account the actual band-limited 'noise' $N(t)$, show an essential agreement with the experimental data. It is worth while to observe that the overall friction is now given by $(k-r^*)$, that is, less than under normal conditions. To increase (or ensure!) the stability of the situation, a contrasted texture presented to the upper part of the eye can be coupled in the correct way to the fly. A stripe segment in the lower part of the fly's visual field 'anticoupled' to the fly will then be 'antifixated' with a smaller sigma than before, since the 'friction' has increased from $(k-r^*)$ to (r_2+k-r^*). Correspondingly the dynamics is significantly slowed down. Again the experimental data confirm these expectations.

6.4. *Patterns consisting of two identical elements*

Equation (5.1) also describes the orientation behaviour of the fly towards more complex patterns, if the associated r and $D(\psi)$ are known. Fig. 15 shows the $D(\psi)$ profiles corresponding to two stripe patterns, for different angular separations $\Delta\psi$ of the two stripes. The parameter r (small compared to k, see Reichardt & Poggio, 1975) is obtained under the assumption that the contributions from the two stripes are simply additive. With these parameter values equation (5.1) gives the stationary probability distribution of the error angle ψ with respect to the zero of the pattern (the centre line between the two stripes). However, an analytic solution of the equation, taking into account the non-white spectral properties of $N(t)$, is difficult (see chapter 5). An approximate solution, which illustrates the qualitative effects of the non-white spectral density, is given by equation (5.6). Fig. 16 shows a digital simulation of equation (5.1) and the corresponding experimental histograms indicating the amount of

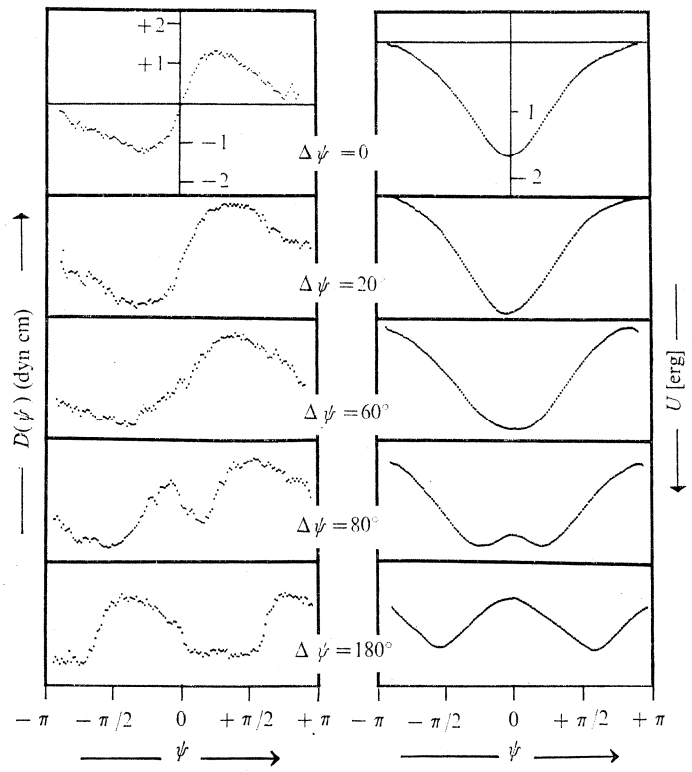

Fig. 15. The 'attractiveness' functions $D(\psi)$ associated to one- and two-stripe patterns: parameter is the angular separation between the black, vertical stripes (5° wide). $\psi = 0$ indicates that the direction of flight coincides with the symmetry line of the pattern, which was oscillated (maximum amplitude $\pm 5°$) around each ψ position. The mean torque was recorded under open-loop conditions. The $D(\psi)$ profiles shown in the left figure are averages of 6–15 individuals and agree well with corresponding measurements performed under the conditions of Fig. 7(*a*). The 'potentials' $U(\psi)$ (right figure) are derived from $D(\psi)$ according to the definition, equation (3.6). Redrawn from Reichardt & Poggio (1975).

time a fly 'gazed' at any part of the patterns. The agreement is satisfactory, since no best fitting is involved in the determination of the parameters (for instance characterizing $N(t)$). Moreover, as discussed by Reichardt & Poggio (1975), the measurement technique introduces some smoothing of the $D(\psi)$ profile which especially affects the theoretical prediction for those patterns in which the two minima of the potential just build up ($\Delta\psi \sim 60°$). It is interesting to observe that the *two* maxima in the theoretical fixation histogram for $\Delta\psi = 60°$ arise from *one* 'potential'

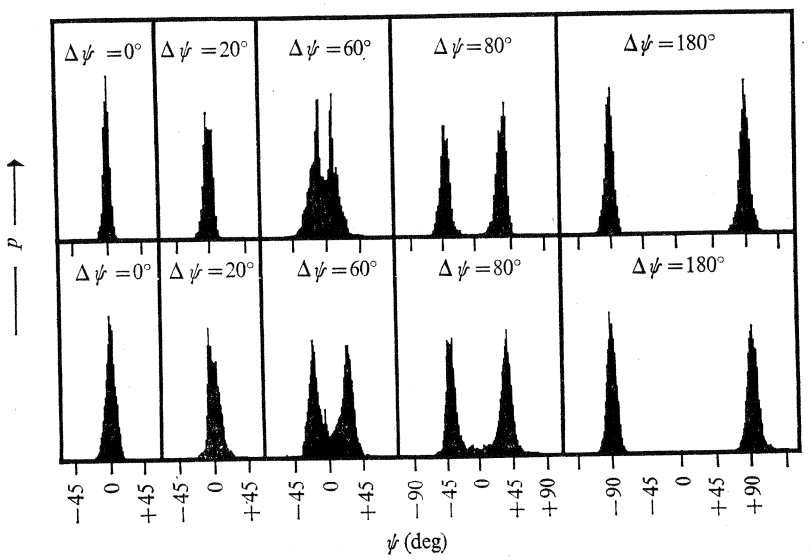

Fig. 16. Distributions of the error angle ψ, during stationary fixation of one- and two-stripe patterns (lower figure). Parameter is $\Delta\psi$ as in Fig. 15. Duration of the experiments, from individual flies, was either 3 min (for $\Delta\psi = 0°$ and $\Delta\psi = 20°$) or 2×3 min. The upper figure shows corresponding histograms obtained from digital simulation of equation (5.1) (with $S(t) \equiv 0$). The $D(\psi)$ functions shown in Fig. 15 have been used in the simulations; the other parameters have the standard values used throughout this paper. The value of Θ/k was $\Theta/k = 8 \times 10^{-3}$ both in the experiments and in the simulations. The simulated time is also equivalent (however, the normalization in the two cases is only approximative). Redrawn from Reichardt & Poggio (1975).

minimum because of the non-white spectral composition of $N(t)$, as shown by equation (5.6). Thus, a two-maxima fixation distribution is observed even when the associated potential distribution contains only one minimum, an effect which may be called an 'early phase transition'. From the point of view of the associated stationary orientation behaviour it is clear that the first three patterns of Fig. 16 are essentially equivalent and in this sense belong to the same class.

6.5. *Tracking of a randomly moving object*

When the object velocity is a random process the error angle $\psi(t)$ is also a random process. Equation (5.1) characterizes completely this tracking situation. Here we want to outline some of the evidence supporting equation (5.1) for these tracking conditions. The first question concerns

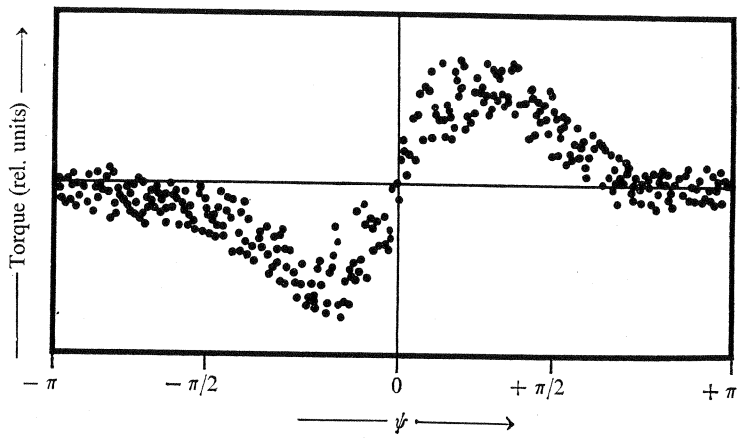

Fig. 17. Scatter diagram showing the relationship between the instantaneous angular error $\psi(t)$ and the fly's torque $F(t)$, during tracking of a black vertical stripe whose angular speed $\dot{\alpha}_p(t)$ was a gaussian 'white' (up to 15 Hz) random process. Because of the small inertia of the fly (negligible Θ), the angular velocity error $\dot{\psi}$ is essentially proportional to F (see equation (2.1)). The satisfactory agreement between this diagram and a corresponding digital simulation (not shown here) of equation (5.1) with the $D^*(\psi)$ of Fig. 7(*a*), support the validity of the approximation, equation (3.4), even under these tracking conditions.

the validity of the approximation equation (3.4), describing the fly's torque response at t as a *function* of $\psi(t)$ and $\dot{\psi}(t)$. It is to be expected that, if the $\psi(t)$ time scale is not longer than the time scale of the torque response, the approximation may fail. While different time scales are certainly involved in *fixation* ($S(t) \equiv 0$), because of the role of the flight dynamics, this must not be true under extreme *tracking* conditions. However, tracking of a black object moving with a gaussian velocity leads to the scattering diagram of Fig. 17, in which the torque response F is plotted against the error angle ψ. It is clear that the approximation of the *functional* R through the *functions* $D^*(\psi)$ and $r^*\dot{\psi}$ is not very precise here. Obviously one must take into account that under these extreme tracking conditions, in which the object is lost very often and $\psi(t)$ changes very quickly, the response of the fly at t actually depends on the recent history of the stimulus. However, the discrepancy is not large; the shape of the scattering diagram essentially agrees with $D^*(\psi)$ of Fig. 7 and simulations of equation (5.1) give similar scattering diagrams, indicating that, up to these conditions, the visual control system of the fly can be described in terms of a position- and a speed-dependent *instantaneous*

response. The large range of validity of this approximation implies that the fly's response is indeed very fast. The $D^*(\psi)$ characteristic appears as a rather stable property of the visual control system of the fly. Later, in Part II, we will discuss the functional mechanisms which underlie its computation.

Further support to this thesis is provided by a recent analysis of the tracking performance when the visual feedback to the fly is delayed (Wehrhahn & Poggio, 1976). Motion of the target (a dark stripe) on the horizontal plane was determined by a zero-mean gaussian angular velocity and the (closed-loop) torque response of the fly was artificially delayed. The average time on target T was measured as a function of the artificial delay ϵ'. The object was considered lost by the fly when the angular error $\psi(t)$ between the direction of flight of the fly and the object reached $\pm 170°$. As Fig. 18 shows, an increasing delay degrades the performance: the larger the delay, the smaller T. With the terms $D^*(\psi(t))$ and $r^*\psi(t)$ delayed by ϵ', equation (5.1) should represent this experimental situation. An approximative solution for T has been derived in the case $\epsilon' = 0$ (Reichardt & Poggio, 1975), but seems otherwise very difficult. Therefore, to check the validity of the model an analogue simulation of equation (5.1) (with the delay) has been carried out. The results are also shown in Fig. 18 and are in satisfactory agreement with the experimental data. Thus, equation (5.1) can also account for delayed tracking. In particular, the function $D^*(\psi)$ of Fig. 7 on which tracking performance critically depends, describes well the position dependent response of the fly, even under the quite extreme conditions of this experiment.

6.6. *Is the theory valid under free flight conditions?*

The essential validity of the phenomenological theory, expressed by equation (3.1), to describe free flight orientation behaviour has been demonstrated by Land & Collett (1974). They have shown that equation (4.1) correctly predicts the time history of the error angle $\psi(t)$ between escaping and chasing male flies (*Fannia canicularis*). Thus, they were able to reconstruct the trajectory of the chasing fly from knowledge of the trajectory of the leading fly. Beside confirming the approximation of the free flight dynamics assumed in equation (2.1), Land and Collett again show that two computations, one transducing position, the other velocity of the target, determine the tracking behaviour of the fly. Apparently because of the 'different' insect (a free-flying free-head

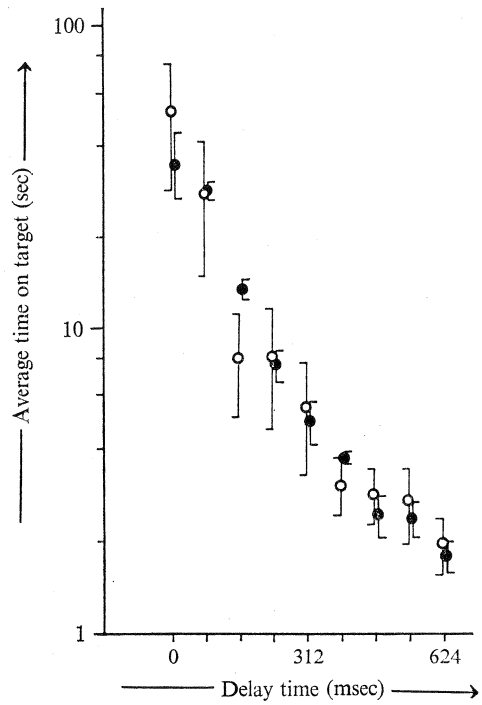

Fig. 18. Tracking performance under artificially delayed response. The data represent the mean time on target (a black vertical stripe) for six female *Musca domestica* (○) and for 4 analogue simulations (with the artificial delay) of equation (5.1) (●). The vertical bars indicate the standard deviation of the mean. The parameter values used in the simulation are those used throughout the paper (see also Poggio & Reichardt, 1973*a*). The target speed $\dot{\alpha}_p(t)$ is a gaussian zero-mean process ('white' up to 15 Hz) with a r.m.s. amplitude of about 50°/sec. From Wehrhahn & Poggio (1976).

'chasing' *Fannia* male) the $D(\psi)$ term has in this case a shape different from the one of Fig. 7(*a*) (for female *Musca domestica*); in fact their scattering diagram (Fig. 6*a*) does not correspond to Fig. 17.

In summary, these results provide critical evidence that our phenomenological theory which describes the artificial closed-loop situation of our experiments applies equally well to free flight conditions.

The biological importance of this point should not be underestimated: it means that the visual control system of the fly as it is unravelled through our artificial closed-loop and open-loop experiments, also accounts for the '*natural*' free flight orientation and tracking behaviour of flies. Furthermore, support is provided by more recent observations in *Syritta* (Collett & Land, 1975*a*).

7. Movement and position responses associated to arbitrary patterns

The phenomenological theory predicts quantitatively natural closed-loop orientation behaviour of the fly (in one dimension) from knowledge of the open-loop responses $D(\psi)$ and $r\dot{\psi}$, associated to a pattern. The examples of the previous chapter provide enough grounds for believing the theory to be a satisfactory description of the visual control system of the fly. The basic problem which arises now is how to determine the terms $D(\psi)$ and $r\dot{\psi}$ for arbitrary patterns. Clearly the problem essentially concerns the functional properties of the nervous interactions which compute the position and the velocity terms. In this sense it is closer to the functional level of our studies of the visual control system of flies and should be dealt with in Part II. However, we will outline here a first-order approach to the problem for two reasons. First, this is required for the completeness of the phenomenological theory. Secondly, it links the phenomenological level (Part I) with the computational and functional level (Part II) of our approach. A complete knowledge of the interactive structure underlying position and movement computation could provide the fly's response for every visual pattern and, through equation (5.1) or modifications of it, the orientation behaviour of the fly in a variety of conditions. We outline here an empirical rule which predicts the fly's response to an arbitrary pattern. A discussion of its range of validity and its failure in specific cases gives insights into the interactive mechanisms underlying the fly's visual control system and shows the need of the 'interaction' approach of Part II, which provides justification for the rule and its limited range of validity.

7.1. *Properties of the fly's response*

Experiments of the type described in section 3.1 suggest that the critical stimuli for eliciting a *visually* induced response under natural conditions are *moving contours* (or edges). This point will be fully appreciated in Part II. As a consequence, a pattern can be often considered equivalent, with respect to the horizontal orientation behaviour, to a sequence of vertical edges or narrow striped segments approximating the pattern contours. In the following we will only consider patterns consisting of vertical black stripes or striped segments.

The term $r^*\dot{\psi}$ associated to a vertical stripe is quite small; moreover it is known that local movement detectors, which can be responsible for

it, are distributed all over the eye and that their contributions approximately summate (Hassenstein, 1968; Götz, 1964; Marmarelis & McCann, 1973). Thus, the additivity of the partial responses from eye regions stimulated by the different parts of a pattern in many cases can lead to a reasonable estimate of r as the sum of the r^*'s associated with the individual segments. A more critical role is played by the terms $D(\psi)$ or $L(\theta)$ carrying, under the assumptions of section 3.4, the position information. In the following, we characterize briefly some properties of these terms.

It should be expected that $D(\psi)$ for a stripe segment depends on the θ location of the object on the fly's retina ($\theta = 0$ designates the equator). That this is in fact the case is shown in Fig. 19; in contrast to the direction-sensitive term the position dependent response is much stronger in the lower half of the eye than in the upper. Other independent experiments have confirmed this finding (Reichardt, 1973, and see Fig. 9 in Part II), which also agrees with the shape of the $L^*(\theta)$ distribution (see Fig. 7). In both cases the upper and the lower part of the eye are not equivalent: while the eye is symmetric around the vertical line dividing the two retinae, there is no such functional symmetry with respect to the equator. Therefore, it seems that with respect to the mechanisms underlying position information a 'functional' fovea may be identified in the lower part of the eye for $-30 \leqslant \psi \leqslant 30$ and $-30° \leqslant \theta \leqslant 0°$. The physiological implications of this point are interesting (see section 6.2 in Part II). Non-trivial behavioural consequences may be implied. If the ability of fixating and tracking is only present in the lower part of the eye, a chasing fly should be mostly flying higher than the leading fly. The leading fly in turn would 'see' the chasing fly's image only in the upper part of the eye. As a consequence, a neural 'fovea' localized in the lower half of the eye could automatically ensure that a 'chasing' fly may not be chased by the 'escaping' fly. However, this conjecture may be weakened by various considerations. Another possible explanation will be suggested in section 5.3 (Part II).

The dependence of $D(\psi)$ on the size of a small vertical segment located in the middle of the lower half of the eye has also been investigated. While it is clear that the maximum attractiveness decreases in a nonlinear way with the size of the segment, the slope does not change to the same extent. On the other hand when a black stripe is embedded in a texture of increasing contrast the *slope* of its $D(\psi)$ decreases (Virsik & Reichardt, 1976). More extensive and detailed experiments of this type should provide insights into the type of mechanisms (direct channels *and* lateral

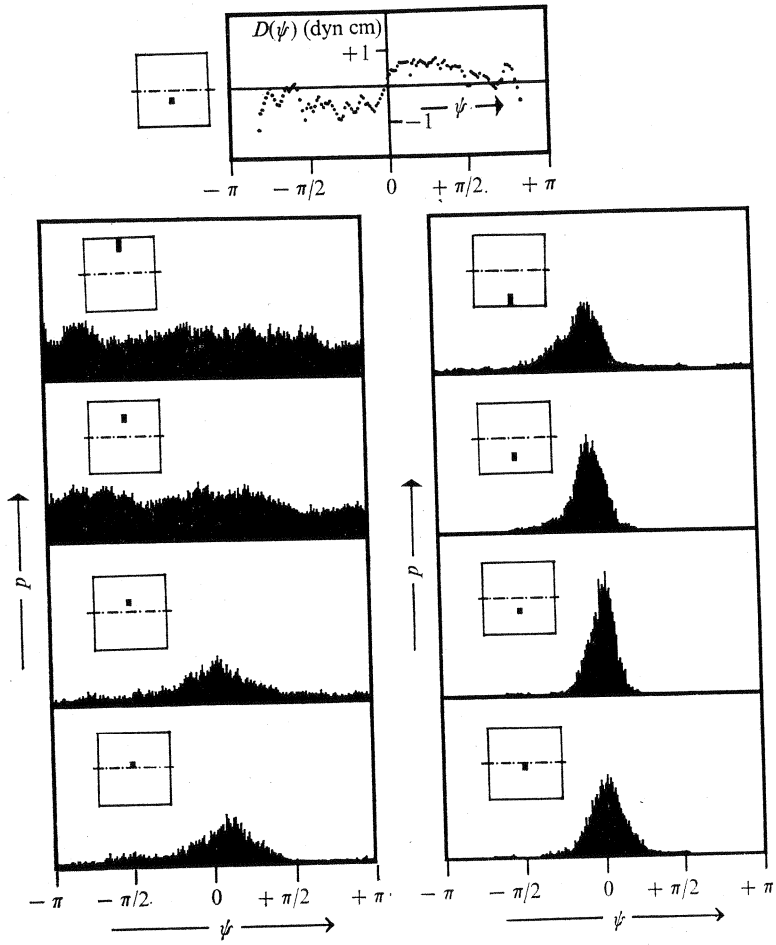

Fig. 19. 'Attractiveness' $D(\psi)$ profile associated to the small stripe segment shown at the left (upper figure). The lower part of the figure shows fixation histograms for small stripe segments, placed (see insets) at different heights θ with respect to the fly's equator (θ = o). The sizes of these segments were such that the number of stimulated receptors was about constant. The fly's equator was about at the level of the horizontal, dotted line. The histograms of the error angle ψ show that stationary, undisturbed fixation is mainly limited to the eye regions below the eye equator. Redrawn from Reichardt (1973).

interactions) underlying the $D(\psi)$ computation (see Part II). It is interesting that contrast inversion of a pattern does not affect $D(\psi)$, *if* the contrast values are no more than 30% (Reichardt, 1973). Thus, a dark stripe on a light background is equivalent to a light stripe on a darker back-

ground. Similarly, since edges or contours are the prerequisites for a visual response, dark edges essentially determine the same fixation behaviour as narrow stripes, if their contrast is not too high. For instance, a 180° wide black 'stripe' (0% transmission) results in a different fixation behaviour from two black vertical stripes, 180° apart, on a white, strongly illuminated, background (the overall flux of light is different in the two cases). However, when the transmission value approaches about 50%, the stationary fixation behaviour is essentially similar in the two cases (Reichardt, unpublished). Therefore, at high contrast values these simple equivalences do not hold, perhaps because of adaptive and phototactic effects (see also Part II, chapter 6). These results are in agreement with ethological observations of Vogel (1957).

7.2. *The superposition 'rule'*

Reichardt (1973) has suggested that the $D(\psi)$ attractiveness of patterns consisting of two or more narrow stripe segments could be derived from the superpositions of the attractiveness profiles of each component independently (with the appropriate angular shifts). A few experiments confirmed the qualitative validity of this 'superposition rule' both for horizontal (Reichardt, 1973) and vertical (Wehrhahn & Reichardt, 1975) fixation in so far that the maxima in the stationary gaze histograms can be predicted from the position of the minima in the potential obtained by superposition of the single potentials. This 'rule' explains, quite simply, phenomena like the appearance of two minima in the two stripes potential (see Fig. 15). As it will be discussed later (section 8.5), the simple superposition rule coupled with the phenomenological equation, can account for non-trivial orientation towards relatively complex patterns. However, the quantitative validity of the superposition 'rule', especially for pattern elements in close proximity, looks rather unrealistic (imagine the limiting case of two superimposed stripes!). We have investigated this problem for the simple case of two-stripe patterns, comparing the $D(\psi)$ of Fig. 15 with the ones obtained through shift and superposition of the one-stripe potential. The conculsion is that, while the qualitative agreement is satisfactory, the quantitative details are not, for small stripe separations. The simplest explanation, a motor output saturation which bounds the attractiveness values, can be ruled out by two arguments (Reichardt & Poggio, 1975). The first one is that the slope of $D(\psi)$ around zero does not increase for neighbouring stripes. The second rests on measurements of $D(\psi)$ associated to small stripe

segments, where motor output saturation should be less significant. The alternatives left are functionally equivalent to the existence of lateral inhibitory interactions, affecting the attractiveness of the pattern. It is clearly conceivable that this *functional* lateral inhibition may be actually mediated through some kind of semilocal saturation (e.g. in small-field neurons). For instance, consider the somewhat different case of the attractiveness ($D(\psi)$ values) associated to narrow segments (or edges) of increasing height: the attractiveness of the object at a given ψ does not increase proportionally with the number of stimulated receptors (on the vertical coordinate θ). Since motor output saturation can be disregarded, at least in some cases, the only possible explanation rests on *functional* inhibitory interactions between ommatidia with the same ψ but different θ. There are two possible implementations of these functional interactions: the first is saturation in the ψ channel (or neuron) which collects inputs from receptors at different θ, the second consists of neurophysiological inhibitions between signals from receptors belonging to the same vertical 'slit'. The two alternatives are, at our functional level, completely equivalent and correspond (see Part II) to the existence of both *functional* inhibitory interactions between inputs (crossinteractions) *and* excitatory channels (selfinteractions) from the individual inputs. The question can be better grasped in the framework of Part II and will be briefly discussed there, in connection with the neural mechanisms which possibly underlie the nonlinear functional interactions responsible for the position and for the movement computation.

7.3. *Restrictions of the superposition 'rule'*

The quantitative failure of the 'superposition rule' implies that interactions between input channels affect the 'attractiveness' of a pattern, when the angular distances separating the pattern elements are not separated enough. As we will discuss later these inhibitory lateral interactions might strongly and selectively depend on the spatio-temporal mapping of the specific pattern onto the receptor array, modifying the simple $D(\psi)$ computation. However, for larger object separation (*certainly* for more than 80°) the superposition rule seems to represent a satisfactory approximation. If this also holds for other dynamic degrees of freedom, a 'transitivity' law for spontaneous pattern preference behaviour in flies would apply (Götz, 1971; Poggio, 1974). In other words, if objects A and B are shown to the fly and A is preferred to B while B is preferred to C, A *must* be preferred to C.

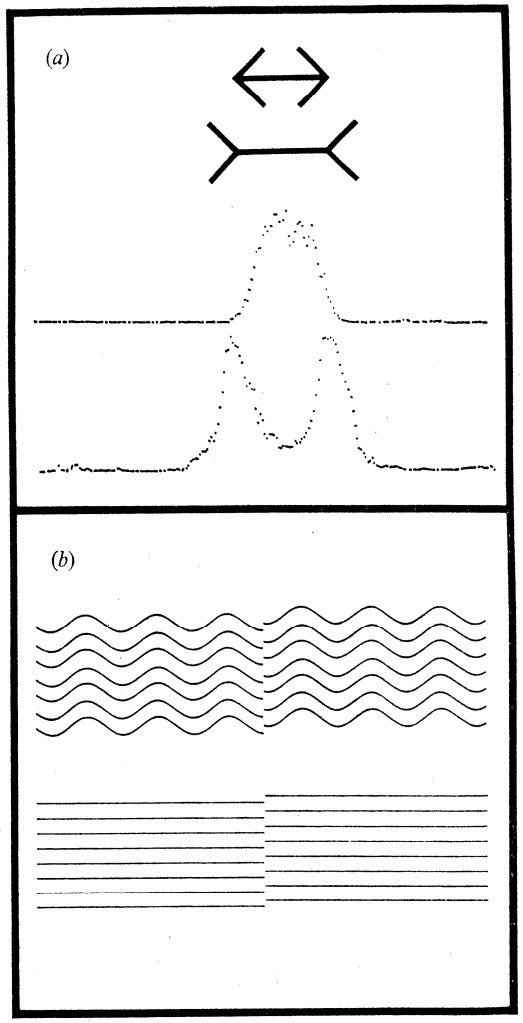

Fig. 20. (*a*) The Müller–Lyer figures (upper part). In the experiment shown here the angular length of the horizontal line, as seen by the fly's eye, is 60°. Histograms of the fly's gaze on the two figures are shown in the lower part of (*a*). The histograms extend from $-180°$ to $+180°$ and show the fraction of time the fly gazed at any part of the two figures. The potential profile $U(\psi)$ associated with each of the two figures can be obtained, in first approximation, by superimposing the contributions of the various line segments. Oblique segments are, in this respect, practically equivalent to their vertical projections. Thus the appearance of the two maxima depend on the angular separation of the two vertical segments, corresponding to each one of the Müller–Lyer figures (compare Figs. 15, 16 and equation (5.1)). The histograms show clearly that the fly's gaze corresponds to our eye movements

In summary, the attractiveness profile of an 'arbitrary' pattern can be derived by superimposing the movement responses and the position responses elicited by the various components, provided that their angular separations are sufficient. It is very important to realize that the central role of the one-stripe $D^*(\psi)$ in our theory, essentially rests on the validity of the superposition 'rule'. Since, with respect to the horizontal degree of freedom, a pattern can be approximately represented by vertical narrow segments, the overall response can be obtained by superimposing the segment responses. Thus, edges or narrow vertical stripe segments are, when superposition holds, the basic *features* of a pattern and the associated $D^*(\psi)$ profile represents a fundamental element of the theory (for orientation in the ψ degree of freedom).

However, for figures with small spatial separation this rule quantitatively fails: nonlinear, inhibitory interactions affect the 'attractiveness' computation and the various pattern elements do not simply give additive contributions. Under these conditions vertical edges or segments are not the basic features to which every pattern can be reduced through the superposition rule. The effects of the elements of a pattern are not independent and the spatio-temporal configuration of two nearby elements act as a new 'feature', independent from other pattern elements outside the range of the lateral interactions. Part II will give a dramatic example of this, involving 'figure-ground' discrimination.

Despite its limited range of quantitative validity, the superposition rule is quite effective as an heuristic tool† to predict the qualitative orientation behaviour of the fly for a large class of patterns. A number of recent experiments from our laboratory support this claim. An illustration is given in Fig. 20: the way the fly 'gazes' at the various figures can be predicted by the heuristic rules outlined in the previous paragraphs.

† Part II clarifies the range of validity and the foundations of the superposition rule.

(Yarbus, 1967) as well as to our subjective (and illusionary) evaluation of the segment length. From Geiger & Poggio (1975*b*).

(*b*) A fly fixates (in the set-up of Fig. 3) the 'illusionary' vertical line arising at the boundary between the two sets of parallel horizontal lines of the ~~upper~~ pattern. However, there is *no* fixation of a similar 'illusionary' vertical line in the ~~lower~~ pattern. The histograms of the fly's gaze are not shown here (Poggio & Geiger, unpublished). The phenomenological theory correctly predicts these results (see chapter 7).

H lower
H upper

8. Discussion

8.1. *The central thesis of the theory*

Perhaps the most significant aspect of the phenomenological theory is the demonstration that (closed-loop) orientation behaviour can be quantitatively predicted from knowledge of the open-loop response of the fly. The phenomenological equation (5.1), which takes into account the dynamics of flight, links (open-loop) information processing in the visual system with the natural orientation behaviour.

The critical role of this point for an understanding of the visual control system of the fly is clear. It means that one can consider the computations performed on the visual input by the nervous system as independent from the motor loop being 'open' or 'closed'. In other words, knowledge of open-loop information processing, as measured in behavioural (or electrophysiological) experiments, can predict, through the phenomenological theory, the (closed-loop) 'natural' orientation behaviour. Furthermore, it suggests that an analysis of the computations performed under open-loop conditions, as it is very often the case, is in fact completely sufficient for an understanding of the behaviour. This represents an essential prerequisite for the approach described in Part II.

Interestingly, the 'Reafferenz-Prinzip' (Mittelstaedt, 1971) seems not to be necessarily required at the level of the behaviour studied here. We have not yet seen any example of (closed-loop) orientation behaviour, which cannot be accounted for in terms of open-loop responses. Even the 'figure-ground' discrimination, described in Part II, is not a strict 'closed-loop' phenomenon as one would expect if reafferent mechanisms would be present, but it reflects open-loop computations. In a 'natural' situation these computations allow the fly, without the need of 'reafferences', to distinguish between self movement and object movement. On the other hand it is possible that reafferences of some type may play a role if head movements are also taken into account.

8.2. *Separation of the fly response*

A critical assumption leads to the separation of the fly's response in a visually induced component *and* in a 'noise' term $N(t)$, essentially independent from visual input. The arguments of section 3.3 imply that the visually induced response can be further decomposed into a *position* dependent *and* a *velocity* dependent component. Many experimental data support the validity of these *conceptual* decompositions and indicate

that the visual control system of the fly rests on two main computations, one converting position information into torque ($D(\psi)$), the other converting velocity into torque ($r\dot{\psi}$). An analogous decomposition holds for the lift response underlying height orientation (Wehrhahn & Reichardt, 1975). In Part II we will characterize the functional properties of these computations. An important question here concerns the physiological implications of the separation of the fly response into the three parts: $N(t), r\dot{\psi}, D(\psi)$. In a strict sense the separation is a first order, conceptual approximation and cannot, by itself, imply any corresponding physiological separation. However, it may provide suggestions about the structural organization of the underlying nervous network. First, the independence of the term $N(t)$ from visual input suggests the existence of a 'noise' channel, separate from the channels carrying position and movement information to the motor output. This simple conjecture is supported by recent electrophysiological evidence, part of which we have already mentioned (see section 3.3). Moreover, fibres in the visual ganglia, for instance in the lobular plate, show a noise-free, visually induced activity. On the other hand, comparable recordings from the cervical connective, which links the brain with the thoracic ganglion, show the presence of spontaneous activity in addition to the visual induced activity (K. Hausen, R. Hengstenberg, personal communications). The physiological localization of the' noise' channel is clearly an interesting physiological question. Is the 'noise' simply the superposition of many 'gating' signals from the brain or is there a channel conveying a complex 'scanning algorithm', which we interpret as noise? Various possibilities are conceivable, including the (unlikely) presence of a kind of neural 'noise generator'; only further physiological work can clear these points. It is, however, quite satisfactory that, in the case of $N(t)$, the conceptual separation, suggested by the phenomenological theory, seems to reflect an actual physiological separation.

Secondly, we consider the terms $r\dot{\psi}$ and $D(\psi)$. Physiological suggestions and inferences will be discussed in detail in Part II. However, a few points should be introduced here. The most simple conjecture is that two systems compute separately the two terms. In Part II we will show that functionally distinct types of interactions underlie the computation of movement and position dependent response. The hypothesis seems also confirmed by a series of experiments on some *Drosophila* mutants recently found (Heisenberg & Götz, 1975; Heisenberg, 1976). The idea is also supported by the fact that, while the movement dependent response

can be elicited by stimulating the upper as well as the lower part of the eye, this is not the case for the position dependent response (Reichardt, 1973). Fig. 19 shows that $D(\psi)$ is quite small in regions of the eye above the equator. Thus, the movement computation is homogeneous with respect to ψ and θ; the position computation, on the other hand, is essentially nonhomogeneous with respect to ψ and θ. As a matter of fact, the localization of the 'attractiveness' $D(\psi)$ in the lower part of the eye, its linear behaviour between $-30°$ and $+30°$, together with the shape of $L^*(\theta)$ (zero-crossing *below* the equator), suggest the existence of a *functional* fovea in the eye region $-30° \leqslant \psi \leqslant 30°$, $-30° \leqslant \theta \leqslant 0°$ (Wehrhahn & Reichardt, 1975). It is quite interesting that the distribution of the horizontal giant fibres of the lobula plate indicates, for a roughly corresponding region of the visual field, the existence of a neural fovea (see section 3 and Pierantoni, 1974; Hausen, 1976; Strausfeld, 1976*b*). No real optical fovea can be found in *Musca*, even if the facet size increases from back to front, in males more than in females (Braitenberg & Hauser-Holschuh, 1972; Beersma, Stavenga & Kuiper, 1975).

The spatial inhomogeneity of the $D(\psi)$, $L(\theta)$ computation compared to the apparent homogeneity of the $r\dot{\psi}$ computation may represent an important key for anatomical and electrophysiological identifications of the underlying nervous structures. The solution of this problem is a prerequisite for an understanding of the visual ganglia. For instance, is the lobula plate essentially involved in the spatial integration of the direction selective optomotor response (the term $r\dot{\psi}$) and is position information (the term $D(\psi)$) processed somewhere else? Or rather are both components already present in the signals leaving the lobula plate?† These questions are now in the range of electrophysiological techniques and the first answers should be forthcoming.

An important point connected to position and movement computation is the very small delay which is involved: behavioural experiments (Land & Collett, 1974; Buchner & Reichardt, 1976) suggest a dead time in the fly response smaller than 30 msec. The exact evaluation of the dead time involved in the fly response is, however, quite difficult. For instance, one should not confuse dead time with time constants of the dynamics of the process. Moreover, conclusions drawn from closed-loop measurements must be taken with great care: for instance, crosscorrelations between

† The lobula plate (the smaller of the two third-order 'ganglia') seems a typical specialization of flying Diptera, perhaps serving their navigatory requirements: other insect species, e.g. locusts, do not have a lobula plate.

$\psi(t)$ and $\dot{\psi}(t)$ in closed-loop (Fig. 8, Land & Collett, 1974) actually depend on the numerical value of parameters like r and not only on the actual delay. However, closed- *and* open-loop measurements as well as simulations of equation (5.1) support a delay value around 25 msec (Buchner & Reichardt, 1976). In connexion with the usually slower dynamics of vertical fixation (equation (3.9)) the lift response delay seems to be larger, in the order of about 50 msec (C. Wehrhahn, personal communication).

A rather small delay value is also suggested by electrophysiological data. For high light intensities (as in most of our experiments) the latency of receptors R1–6 can be about 4 msec in the lamina (Järviletho & Zettler, 1970, 1971, 1973), where the latency of the L1–L2 fibres is about 5 msec. The conduction time from the lamina to the medulla can be estimated to be in the order of 2–4 msec from electrophysiological (Scholes, 1969) and anatomical considerations (Boschek, 1971). R7–R8 bypass the lamina: however, since their diameter is about half the diameter of the R1–R6 and L1–L2 cells, the overall delay involved in the R7–8 system should be of the same order as the one associated to the R1–R6, L1–L2 system. Three more milliseconds may be involved between the medulla and lobula or lobula plate (two synapses and conduction time). As a matter of fact the latency of some giant fibres in the lobula plate can be as little as 12 msec (Hausen, 1976). Conduction time and maximum rate of the non-fibrillar N-muscles (Heide, 1975) put a lower limit of about 11 msec to the time needed for the lobula plate – flight muscles transduction, giving a (minimum) estimate of about 23–25 msec for the overall delay between a visual input and a motor torque output.

These figures imply, together with the behavioural data, that the amount of serial processing involved in the computation of the orientation response of the fly is relatively small. This, in connexion with the parallel and repetitive organization of the system, represents an important argument for the 'interaction' approach of Part II.

8.3. *The role of the 'noise' $N(t)$*

The 'spontaneous' torque output represented by $N(t)$ is characterized by the phenomenological theory in stochastic terms. Of course, this does not imply by any means the existence of a 'noise' generator in the brain of the fly. The stochastic approach only reflects our hypothesis of 'ignorance' about $N(t)$. In principle, a precise knowledge about the internal states of the fly could allow a 'deterministic' treatment of the

spontaneous behaviour $N(t)$. This would be for instance the case if $N(t)$ would arise from the superposition of various centrifugal gating signals, reflecting 'intentions' and 'moods' of the fly. It is possible that our hypothesis of 'independence' of $N(t)$ from visual input is, strictly speaking, only a first order approximation and that further studies will reveal some degree of dependence on the visual input.† In particular, in a mathematical treatment of the head-free situation, amplitude and frequency distributions of head saccades (when present) would probably depend on visual input (Poggio, 1972). Thus, the visually induced response would not simply add to the noise term. Rather, it probably 'gates' and 'rearranges' the stochastic occurrence of saccadic head movement. However, under our experimental conditions the term $N(t)$ cannot be neglected in the phenomenological description of the (fixed-head) orientation behaviour. It is always present and determines many important aspects of fixation and tracking. Without it, the histograms, shown in this paper, would be very similar to a delta function. A *tracked* moving object would be never lost and the spontaneous behaviour, in absence of any pattern, would amount to flying continuously in *one* direction. Of course, a satisfactory description of the orientation behaviour can be given also in terms of expected values (for instance, the average error angle during tracking, see Figs. 12–14), especially if the effects of $N(t)$ are of the same order as the experimental errors. In this sense the role of the noise is important but certainly not critical.

What then is the *function* of the 'noise' behaviour $N(t)$? Similar questions are usually asked about tremor and microsaccades in human eye movements (see for instance, Steinmann *et al.* 1973). Clearly a complete answer in the fly case requires the consideration of head movements: the role of $N(t)$ must be seen in this context. However, it seems interesting to speculate about the possible function of the spontaneous behaviour, with the restriction that our inferences are based on head-fixed experiments in the set-up shown in Fig. 3. A possible function of the spontaneous behaviour $N(t)$ is the necessity to avoid stabilized retinal images, which quickly fade and are not any more 'seen' by the fly (see also Part II). Clearly this problem arises *only* for fixation of stationary objects or tracking of targets moving at *constant* angular velocity. Another possible, more important role of $N(t)$ is the 'scanning' of the visual environment. If $N(t)$ did not exist, or were too small, the fly would

† For instance, it may be that part of the effect shown in Fig. 10 can be interpreted as 'noise suppression' by optomotor response.

remain 'locked' into any, even very small, potential well 'generated' by a panorama. $N(t)$ takes care of this problem allowing the fly to 'jump out' of a potential well and thus to 'explore' the whole panorama. If this is so, the power A of $N(t)$ (e.g. section 3.1) determines to which extent precision of fixation compromises with the exploration of the environment (under our experimental conditions). Some dependence of the $N(t)$ power on states of activity of the fly is, for instance, likely (cf. Götz, 1975*a*). As we will discuss later the fluctuation term $N(t)$ plays a critical role in the phase transitions occurring in the stationary orientation behaviour.

Clearly it is possible to push this kind of arguments even further. The fluctuation term $N(t)$ plays in the fixation process the same role which mutations play in evolution (see for instance Eigen, 1971): it is a random trial and error scanning procedure which finds, between all minima of the potential associated to a panorama, the absolute minimum in other words the most attractive, the 'best' object. One point must be mentioned here. It is possible to show that the phenomenological equation, equation (5.1), represents an algorithm for finding the optimal (in the least-square sense) match between a visual pattern and a 'memorized' pattern $-U(\psi) = -\int D(\psi')\,\mathrm{d}\psi'$. This interpretation of the tracking algorithm can 'explain' a number of related behaviours (Collett & Land, 1975*a*, *b*; Scharstein, 1974) and also indicates a possible deeper meaning of the fixation behaviour. We shall come to this later.

One point is worth stressing again. Extension of the phenomenological theory to describe head movements is possible. Saccadic-like head movements can be included in the phenomenological equation (Poggio, 1972). In addition to the observations of Kirmse & Lässig (1969), Land (1973), and Liske (1976), further experimental work is necessary to characterize more precisely and more completely the saccadic control system in the fly (Geiger, in preparation): stimulating suggestions about its functional organization are (possibly) provided by work on vertebrates (Bizzi *et al.* 1972; Morasso, Bizzi & Dichgans, 1973). A quantitative experimental characterization should allow either a stochastic Fokker–Planck formulation analogous to the one presented here or an equivalent mathematical analysis (Sancho, 1969). The problem is technically more difficult but we do not expect basic qualitative differences in the description of the fixation and tracking process. Moreover, head-free flies do not show a behaviour qualitatively different from head-fixed flies, suggesting that our fixed-head description may not need any drastic change to account for the free-head situation

(see Reichardt, 1973; Virsik, 1974). It is rather likely that body rotations and head movements are independently controlled by the visual input with peripheral feedback loops providing the necessary coordination.†

8.4. *Validity of the theory and possible extensions*

8.4.1. Statistics enters into the theory outlined here in two different ways. First, as we have discussed earlier the continuous presence of a fluctuation process $N(t)$ dictates a stochastic approach; in this context, one can strictly speak only about (time-dependent) probability distributions of error angle $\psi(t)$. Secondly, individual variability between flies implies that the parameter values used in the phenomenological theory are *average* values; thus a quantitative comparison between theory and experiments requires values averaged from a few flies. For instance, quite an individual variability is found in the shape and in the values of the function $D^*(\psi)$. Furthermore, some variability of the attractiveness profile $D^*(\psi)$ also seems to be present in individual flies. Even if not critically important for the behaviour described in this paper a certain amount of plasticity is surely present (Geiger, 1975).

8.4.2. The biological validity of the theory has been demonstrated also in the observations of Land & Collett (1974) of the chasing behaviour of *Fannia* males. They have been able to confirm at the same time the approximation of the flight dynamics used in the closed-loop experimental set-up of Fig. 3 *and* our description of the visually induced response of the fly (equation (5.1)). It is interesting to observe that most of our experiments have been performed on female *Musca domestica* (a few experiments with male *Musca* have given equivalent results), while the chasing behaviour studied in *Fannia* by Land and Collett is performed only by males. Since the type of visual control system involved in the two cases is essentially the same, it seems likely that we are dealing in both cases with the same neural mechanisms, simply with a different sensitivity to size and to speed of the target. Thus, we do not expect to find male-specific 'chasing' neurons as postulated by Collett & Land (1975*a*). Possibly the transient higher sensitivity required by chasing can be only triggered in males by an ensemble of peripheral and central gating signals: if it is so, it may be quite difficult to observe chasing in our artificial closed-loop set-up, where many degrees of freedom are blocked, the target distance is fixed and some peripheral sensory feedbacks are inactive.

† The hairs around the neck are certainly involved in this coordination, modulating the torque output of the wings (Liske, 1976).

It is interesting to observe that an approximation of the fly's response in terms of a velocity and a position *function* (section 3.3) critically depends on the time scale determined by the specific flight dynamics. This point represents more than a mathematical curiosity and suggests an 'evolutionary' match of the visual control system of the fly to the flight dynamics.

8.4.3. The theory and the experiments outlined in these two papers are of course restricted to a specific part of the orientation behaviour of female flies *Musca domestica*. They do not exhaust the complexity of the visual behaviour of flies. For instance, hoverflies (Collett & Land, 1975*a*) show a rich set of various different 'procedures' used to control the flight course. A formal description of such a complex behaviour, including the switching from one behavioural 'frame' to another, is not yet available. However, our phenomenological theory seems so far to account *completely* for the orientation behaviour of female *Musca*, in one degree of freedom (either ψ or θ). Moreover, the same formalism essentially describes behaviour of flying (Heisenberg, 1972; Heisenberg & Götz, 1975; Zimmermann & Götz, in preparation) and walking (Horn & Wehner, 1975) *Drosophila melanogaster*, chasing in *Fannia*, smooth tracking in hoverflies, visual fixation in walking *Tenebrio molitor* (Varjú, 1975) and possibly object fixation in flying locusts (Baker, 1975).

8.4.4. The most obvious limitation of the phenomenological theory is its restriction to one dynamical degree of freedom. So far both the rotational degree of freedom, ψ, and the vertical one, z, have been described *separately*. It is not yet clear whether orientation behaviour in the two degrees of freedom simultaneously can be accounted for by the two equations (3.8) and (3.9). In other words it is not clear whether the torque response of the fly depends in a non-trivial way on θ and $\dot{\theta}$ and whether the the lift response depends on ψ and $\dot{\psi}$ (of course $D^*(\psi)$ is 'trivially' parametrized by θ as well as $L^*(\theta)$ by ψ). However, we conjecture that the two degrees of freedom are independent and that equation (3.8) and equation (3.9) may describe a two-dimensional orientation behaviour. As a matter of fact the direction sensitive optomotor response is known to depend, as torque, on ψ motion and, as lift, on θ motion (Götz, 1968; Wehrhahn & Reichardt, 1975). Moreover, the type of computations underlying the $D^*(\psi)$ computation (self-interactions, see Part II) seems to exclude the possibility of a complex θ dependence. In other words, it seems clear that, at the level of a first-order approximation, the position information is mediated by $D_\theta(\psi)$ for the torque and by

$L_\psi(\theta)$ for the lift. The underscripts indicate the parametrization of $D(\psi)$ on θ (see Fig. 19) and the (unknown) parametrization of $L^*(\theta)$ on ψ. It is interesting to compute what the ψ and θ parametrizations of $L(\theta)$ and $D(\psi)$, respectively, should be in order that position dependent torque and lift responses can be derived from a 'potential' $U(\psi, \theta)$. The required integrability conditions, trivial in one dimension, are quite restrictive in two dimensions. For instance, the torque $D^*(\psi)$ should depend on θ as $-U^*(\theta)$ of Fig. 7(*b*), and the lift $L^*(\theta)$ should depend on ψ as $-U^*(\psi)$ of Fig. 7(*a*). The question is still open to experimental test. However, there seems to be no special reason (like a conservation principle in physics) requiring this to be true (see Wehrhahn & Reichardt, 1975).

In summary, it is possible that the two equations, equation (3.8) and equation (3.9), suffice to describe the orientation behaviour in the two dimensions ψ and θ, at least for patterns for which the superposition rule is valid.

8.4.5. Another important degree of freedom which is not explicitly taken into account by equation (5.1) is the translatory one. The importance of translatory movements of a free fly for influencing its navigation has been made very clear by recent studies of Götz (1975*a*) with *Drosophila*. His approach takes into account that the output of movement detectors in the visual system of insects is equivocal with respect to the speed of the 'panorama' relative to the eye (e.g. zero response at both zero and infinite speed). Additive decomposition of the stimulus into translatory and rotational components is not feasible. A translatory bias may even change the sign of the rotatory response of an insect. In terms of the orientation equation (5.1) (see also section 6.2) translatory movement may be taken into account through an additional term $r_2(v, \dot{\psi}_b)$, reflecting the movement response induced by the background ($\dot{\psi}_b$ is the angular error velocity of the fly relative to the environment and $\dot{\psi}_b = \dot{\psi}$ if $S(t) = 0$). The effect of the translatory bias is parametrized by the translatory speed v. Let us assume, for instance, that $r_2(v, \dot{\psi}_b) \simeq r_2(v)\dot{\psi}_b$ (for small $\dot{\psi}_b$). Then, because of general properties of the computations responsible for movement detection (Götz, 1975*a*; see also Part II), $r_2(v)$ may become negative for increasing values of v. Instabilities of the orientation behaviour may thus arise from this negative 'friction' Together with the $D(\psi)$ term associated to a possibly complex pattern, this would lead, as a detailed analysis shows, to a quite rich dynamical behaviour characterized by a series of new stable and

unstable situations, determined by the inter-play of $r_2^*(v)\,\dot{\psi}_b$ and $D(\dot{\psi})$. However, it seems necessary to gain some more insights in the fly's control of translation, before approaching this problem.

8.4.6. The phenomenological theory must also be extended to include the head movements, which are eliminated in our experiments. As we have mentioned before, the body-head control system of the fly shows similarities with the human oculomotor system (Poggio & Reichardt, 1973*a*; Collett & Land, 1975*a*), and may in this sense represent a very interesting model system. An interesting question in this connexion is whether the analogy concerns only the organization of the control system or extends to the computations extracting position and movement information (see Part II).

As a matter of fact there are a number of similarities between fly's and human eye's fixation of stationary or moving targets. In both cases there is a continuous 'noise' production (tremor and saccades in the human eye), in both cases stationary targets are not perceived. Tendencies for fixation of patterns by human observers (Richards & Kaufman, 1969) show other suggestive analogies. The observer's eyes point towards a position within the pattern, near the boundaries, if the contours exceed an angular separation of about 5°; otherwise the average point of spontaneous fixation is located near the centre of gravity of the pattern. In an analogous way the average direction of gaze of a fly is towards the centre of gravity of a two-stripe pattern if the angular separation of the stripes is less than 40–60°, whereas it is towards the boundaries (*inside* the pattern) for larger separation angles. The phenomenon is correctly accounted for by the phenomenological theory. An essentially equivalent situation arises with the Müller–Lyer figures of Fig. 20(*a*). Again in this case the human eye movements (Yarbus, 1967) are similar to the fly's gaze. An intriguing possibility is that our theory may essentially account also for human's eye movements in these situations. As a matter of fact the properties required are quite general and are likely to be true for the human fixation system as well.

Other analogies can be found with respect to tracking performances, for instance in the case of real-time delayed tracking (Smith, 1972; Wehrhahn & Poggio, 1976). In other cases, 'differences' between psychophysical data in humans and behavioural experiments in the fly are seen (see for instance Fig. 20(*b*)). So far, the fly behaves as predicted by the phenomenological theory.

8.4.7. We have mentioned earlier that the pattern induced orientation

behaviour described by equation (5.1) may be interpreted as the implementation of an optimal 'tracking' algorithm based on the maximization of the crosscorrelation between an input spatial pattern of excitation of the receptors and a memorized pattern (in our case $-U^*(\psi)$). Technical applications of it are the phase-locked systems in the fields of coherent communication, radar tracking, synchronization and ground-matched missile guidance. In this sense the orientation equation is an algorithm which finds the maximum of the crosscorrelation function between perceived and memorized pattern. Variations of this algorithm can account for more complex behaviours like stereopsis adjustments in humans (Richards, 1973), distance tracking and homing behaviour in hoverflies (Collett & Land, 1975*a*, *b*) and orientation in ants (Scharstein, 1974). Moreover, the algorithm equation (5.1), which in the orientation behaviour of the fly is implemented from the pattern of excitation of the receptors through a motor loop, may also be a paradigm for more sophisticated information processing in the nervous system (see MacKay, 1972; Marko, 1973). There may be an *evolutionary* continuity between an orientation algorithm and a problem solving or interpretation algorithm. From the evolutionary point of view one may speak of 'centralization of a motor pattern'. These ideas indicate that an understanding of the visual orientation behaviour in insects may be a useful prerequisite for an understanding of information processing in other nervous systems.

8.5. *Phase transitions and Gestalt*

The phenomenological theory, with the approximative superposition rule (section 7.2) describes the mapping of a visual pattern into the orientation behaviour of the fly. Even in the simple situations considered in this paper, restricted to one dynamical degree of freedom, the stationary orientation behaviour towards a structured panorama can be described in terms of a series of *phase transitions*. For instance, in the two stripes case (Fig. 16) a typical phase transition occurs in the stationary fixation distribution for a value of the parameter $\Delta\psi$ (angular separation of the two stripes) of about 40°. For larger $\Delta\psi$ values, the previous stable fixation position $\overline{\psi} = 0$ becomes unstable and two new stable positions appear, determined by the corresponding minima of the potential. The same phase transition is also clearly seen in the 'gaze' distribution during fixation of one of the Müller–Lyer figures (Fig. 20). In fact, since the single stripe potential $U^*(\psi)$ is non-harmonic, the superposition of two or more stripe potentials can easily lead to

'symmetry breakings' (or 'catastrophs', in Thom's (1972) theory) with regard to the potential minima. It is the addition of the contributions from all channels providing the position dependent response $D(\psi)$, which, as a consequence of their nonlinear ψ-weight, lead to these symmetry breakings. Thus, the nonlinear co-operative superposition of very simple, local computations (see section 4.1, Part II) determines a non-trivial pattern orientation behaviour and underlies an elementary 'classification' of patterns according to their order parameters. Numbers and positions of the minima can be considered as *order parameters* distinguishing different classes of patterns. In fact, the actually small $N(t)$ power maps essentially the minima of the potential profile into the stationary fixation behaviour. Therefore, the stationary orientation behaviour is practically invariant with respect to a class of patterns with the same order parameters. In this sense, the order parameters of a pattern define a kind of *Gestalt* for the fly, since patterns with the *same* order parameters elicit the *same* type of (stationary) *orientation behaviour* (see Fig. 16).

The idea that the co-operative contributions of local computations in the fly's eye may lead to a complex orientation behaviour through the phenomenological equation is very important to our approach. The inclusion of other degrees of freedom in the phenomenological description should determine a much richer pattern of phase transitions and instabilities in the orientation behaviour. For instance, translatory movements may determine, through the direction-sensitive optomotor computation and its interplay with $D(\psi)$ in the phenomenological equation, new 'stable' orientation states. As a simple example, a 'negative' friction ($r_2(v) < 0$), arising from translatory movement with respect to the environment, can lead to stable antifixation of a small object (that is escape from it). The implications of these ideas cannot be overestimated. It means that an open-loop analysis of *local* computations (through either behaviour or electrophysiology) *cannot*, by itself, predict the closed-loop behaviour *without* a 'macroscopic' theory. Co-operative superposition of local computations, as arising from movement detectors and position detectors, can lead to new behavioural modes, new stable orientation states. The difference can be as great as between attraction towards and repulsion from a pattern and does not rely on the properties of the local computations but on their (co-operative) superposition. The underlying reason is that *nonlinear* dynamic systems exhibit a very rich and complex qualitative behaviour, with phase transitions, bifurcations

or, possibly, 'catastrophs'. The analogy with the field of co-operative phenomena in physics is appealing. The ability to predict the closed-loop natural orientation behaviour from knowledge of local open-loop computations (for instance, of movement and position) through the phenomenological theory, does not imply that the closed-loop behaviour is a trivial consequence of these computations. Qualitatively new behaviour can arise from the cooperation of spatially distributed local computations. In this sense the phenomenological theory could become the core of a (non-trivial) theory of spontaneous pattern preference behaviour of insects, where properties of the elementary movement or position detectors (see Part II) and their interplay will have an equally important role. Such a theory can represent a new and more complete approach not only to the navigatory behaviour of insects (following Götz, 1975*a*) but also in the area of pattern discrimination and perhaps pattern recognition in insects. However, we must stress that a computational structure satisfying the superposition rule would be too simple to underlie a sophisticated, form-dependent pattern discrimination behaviour. As a matter of fact, additional local, lateral, nonlinear interactions are suggested by the short range failure of the superposition rule (chapter 8). Clearly a knowledge of the computational properties of these local interactions is an essential prerequisite for a theory of pattern discrimination and actual 'Formensehen' in insects. Part II deals with this point and will show that the computational properties of the lateral interactions restricting the validity of the superposition rule extend at least to the level of figure-ground discrimination and play a critical role in the fly's form and pattern perception.

9. Appendix: Anatomical and physiological background

In this section we attempt to outline some aspects of the anatomy and the physiology of the fly's visual system. The data described here represent the background of our behavioural studies, providing a rough sketch of the fly's brain, at the third level of description ('the circuitry') level. Our highly simplified outline is based on the publications of Kirschfeld (1973), Braitenberg (1972), Strausfeld (1976*a*), and especially Hausen (1976), in which the reader may find more details.

9.1. The central nervous system of flies consists of cerebral and thoracic compound ganglia (controlling the motor output); they are

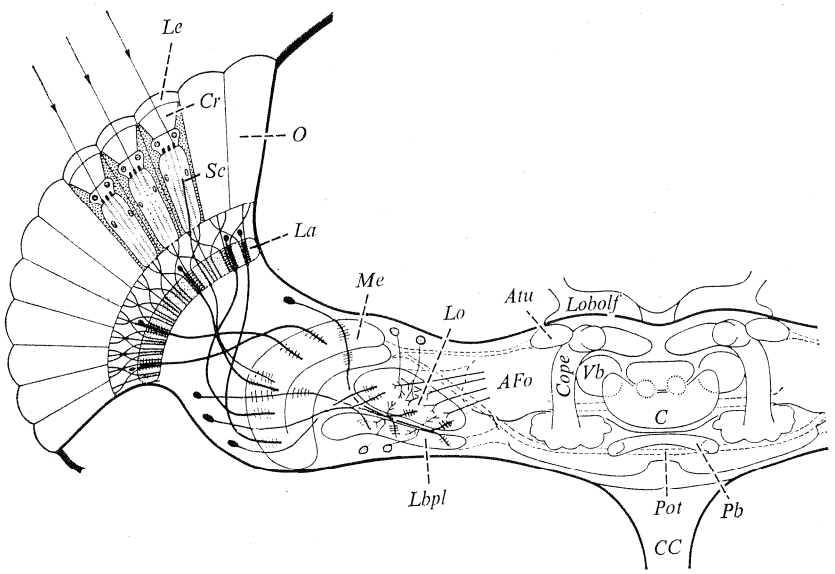

Fig. 21. Cerebral ganglion of *Musca*. The compound eye consists of ommatidia (*O*), corneal lenslets (*Le*), crystalline cones (*Cr*), sensory cells (*Sc*). The first neuropile region is the lamina (*La*), the second one is the medulla (*Me*), followed by lobula (*Lo*) and lobula plate (*Lbpl*). Other structures of the brain are the anterior optical foci (*AFo*), the lobi olfactorii (*Lobolf*), the anterior optical tuberculi (*Atu*), the corpora pedunculata (*Cope*), the ventral body (*Vb*), the central body (*C*), the protocerebral bridge (*Pb*) and the posterior optic tract (*Pot*). The cervical connective (*CC*) connects the cerebral ganglion with the thoracic ganglia. Redrawn from Hausen (1976) and Kirschfeld (1972).

connected through the cervical connective (*CC*). The cerebral ganglion is sketched in Fig. 21 in a horizontal cross-section. All visual functions are localized in parts of the dorsal part of the brain, called the protocerebrum. The main structures of the protocerebrum are the central complex (*C*), the corpora pedunculata (*Cope*), and the protocerebral bridge (*Pb*). The central complex includes various subunits, connected together. It contains visual, chemical and possibly mechanosensory neurons. The central complex is essentially in afferent connexion with most of the other sensorial ganglia in the protocerebrum and in efferent connection with descending elements from fourth-order sensory neuropil and the ventral nerve cord. The central complex is also connected to the protocerebral bridge which also receives inputs from the opticus tuberculus (*Atu*). Probably, the input to the two corpora pedunculata, localized either side of the central body, is mainly chemosensory. The lateral

regions of the protocerebrum contain projection centres of the optic lobes. The posterior optic tract represents one of the major heterolateral connexions of the visual system.

9.2. The optic lobes, behind the eye, consist of four synaptic neuropils: lamina (*La*), medulla (*Me*), lobula (*Lo*) and lobula plate (*Lbpl*). The compound eye of the housefly has about 3000 individual ommatidia (Braitenberg & Hauser-Holschuh, 1972), optically screened (as far as rhodopsin is concerned) from one another by pigment. The representation of the optical environment in the layer of the photoreceptors (rhabdomeres) is determined by the optics of the individual ommatidia, the arrangements of the separated rhabdomeres in each ommatidium and the geometry of the eye. In a cross-section of an ommatidium six rhabdomeres (R1–R6) plus the central rhabdomeres (R7 and R8), are arranged in a typical repetitive pattern. The optical axis of the rhabdomeres differ, so that each rhabdomere receives light from different directions in the optical environment (the ommatidium acts as a small lens eye). In addition, the angular separation of the optical axes of the rhabdomeres matches the ommatidial divergence angles, so that seven (eight) rhabdomeres, each from a different ommatidium, are 'looking' at one and the same 'point' in the optical surroundings (Kirschfeld, 1967; Braitenberg, 1967). As a consequence, optical resolution of the eye is determined by the angle between the optical axes of adjacent ommatidia ($\Delta\phi$).

Apparently the differences in spectral sensitivity between the central (R7–8) and the peripheral (R1–6) rhabdomeres cannot be explained by waveguide effects alone (see Kirschfeld & Snyder, 1975). Every individual rhabdomere is sensitive to linear polarization, due to the localization of pigment molecules in the membrane of the rhabdomere microvilli (Kirschfeld & Snyder, 1975). A single quantum of light is sufficient to elicit an elementary photochemical reaction, which, in turn, triggers an elementary photoreceptor response (Reichardt, 1965, 1970).

The lamina shows a highly periodic columnar structure of elements called cartridges. Every cartridge (there are as many cartridges as ommatidia) consists of a group of interneurons and receives from six ommatidia the six axons of those (peripheral) retinula cells that 'look' at the same point of the visual environment. Thus, a 'point' of the environment is represented in one cartridge, through a complex and highly precise mapping of the retinula axons onto the lamina layer (Braitenberg, 1967; Kirschfeld, 1967; Trujillo-Cenóz, 1972). In each

cartridge the six retinula cells (200 μm long, 2 μm in diameter) are synapsing with at least two (L1–L2 are 250 μm long, 2 μm in diameter) of the five monopolar, second order L-cells. The central retinula cells (R7–R8: 500 μm long, 1 μm in diameter) of each ommatidium cross the lamina without synapsing and terminate in the second optic ganglion, the medulla, after crossing the outer chiasma. The ultrastructure and the synaptology of the retina–lamina complex is well known (Trujillo-Cenóz, 1972; Braitenberg, 1967; Boscheck, 1971; Campos-Ortega & Strausfeld, 1973, 1976; Strausfeld, 1976*b*). Intracellular recordings have been obtained from retinula cells (for instance, Scholes, 1969) and from some of the L cells, identified through dye injections (for instance, Järviletho & Zettler, 1970, 1971, 1973; R. Hengstenberg, unpublished). Intracellular recordings in the retina and lamina of dragonflies have been obtained by Laughlin (1973, 1974, 1975).

An important functional consequence of the retina–lamina connectivity is that an individual cartridge receives information about only one distinct position in the environment. Nevertheless, the cartridges cannot be yet in principle excluded as a possible site for movement detection, since lateral interconnexions between cartridges have been described (Strausfeld & Braitenberg, 1970; Campos-Ortega & Strausfeld, 1973; Strausfeld & Campos-Ortega, 1973).

The outer chiasma between the lamina and the medulla consists of horizontal layers, where crossing of fibres takes place. Frontal cartridges map on to the posterior part of the medulla and vice versa. Recordings of chiasma fibres (Arnett, 1971; Hausen, unpublished data) show a characteristic on-centre off-surround organization, somewhat similar to vertebrate neurons. As yet, no movement sensitive neurons have been found either in the lamina or in the outer chiasma.

9.3. The medulla, probably the most complex of the visual ganglia, also shows a regular columnar structure (Campos Ortega & Strausfeld, 1972*a*, *b*). Every lamina-cartridge maps into a corresponding medulla column; those L cells and R7–R8 cells which represent the same visual point end at different levels of a medulla column and synapse with third-order neurons. Various layers orthogonal to the medulla columns can also be recognized in the various lateral arborizations of amacrine, tangential cells, rich of synaptic contacts. Some superficial tangential cells are connected, through the posterior optic tract, to the tangential cells of the opposite eye, determining a direct medulla–medulla connexion. While most of the efferent fibres of the medulla map into the

lobular complex, some tangential cells connect the medulla with the anterior optical tuberculus and posterior protocerebra.

Electrophysiological data show that a non-trivial information processing takes place in the medulla. A variety of different types of small field neurons can be identified; among them, small-field, direction sensitive 'optomotor' neurons have been found (McCann & Dill, 1969; Collett, 1970; DeVoe & Ockleford, 1976) and the organization of the receptive field (which includes inhibition and excitation) of some of these neurons have also been studied (Mimura, 1972).

9.4. The inner chiasma consists again of horizontal layers: in each layer a first subset of fibres connects (crossed) medulla and lobula, a second one connects (uncrossed) medulla and lobula plate, a third one again connects (crossed) medulla and lobula, while a fourth subset of fibres connects (uncrossed) lobula and lobula plate. Lobula and lobula plate have still a periodic columnar structure (Braitenberg, 1970; Strausfeld, 1976*b*). The distal parts of the two lobulae represent the frontal eye regions and vice versa; the dorsal parts represent the dorsal eye region and vice versa. An ordered mapping determines a unique correspondence between columns in the lobula plate (or in the lobula) and associated cartridges (each one representing one specific point of the visual environment). The columns corresponding to the frontal eye region have the largest volume, indicating the existence of a kind of 'neural fovea' (see section 8.2). A careful analysis of spatial distribution and density of small and giant fibres in the lobula plate may provide, in connexion with the $D^*(\psi)$, $L^*(\theta)$ and $r^*(\psi)$ dependence of the position and movement computations, important links between neural circuitry and behaviour.

Various intercolumnar fibres connect the lobula with the optical foci, the optical tuberculus and the contralateral lobula. Electrophysiological data indicate the existence of small field movement sensitive cells in the lobula (McCann & Dill, 1969; Bishop & Keehn, 1967).

The lobula plate shows, beside small field intercolumnar elements, two sets of giant fibres, first described by Pierantoni (1974) and respectively called horizontal and vertical systems; their axons are connected to cervical connective fibres. Recent studies of the lobula plate have revealed much of the organization of this ganglion, through a very satisfying correlation of histology and electrophysiology (see Hausen, 1976; R. Hengstenberg, unpublished results), various marking techniques and double electrode recordings. The properties of the systems of giant fibres are

now rather well known (Dvorak, Bishop & Eckert, 1975; Hausen, 1976; R. Hengstenberg, unpublished results): at least some of them are large field, direction-sensitive neurons which probably play an essential role in flight navigation. The vertical system is essentially specialized, as postulated by Pierantoni, for the response to vertical motion and the horizontal for horizontal motion. It is still an open question whether other computations (for instance, the lateral, nonlinear interactions described in chapter 5, Part II) beside motion computations are also represented in the activity of the lobula plate fibres. The output of the lobula plate is then mapped into descending neurons which transfer information, via the cervical connective to the motor circuits of the thoracic compound ganglia. Fibres in the cervical connective have been electrophysiologically recorded and intracellularly stained (Hengstenberg, 1973; R. Hengstenberg, unpublished results). A large body of information about anatomy and physiology of the thoracic motor output can be found in Wyman (1966), Nachtigall & Wilson (1967), Wilson (1968), Mulloney (1969), Levine (1973), and Heide (1975).